Topical Administration of Novel FKBP12 Ligand MP-004 Improves Retinal Function and Structure in Retinitis Pigmentosa Models

Araceli Lara-López,[1,2] Klaudia Gonzalez-Imaz,[2–4] María Rodríguez-Hidalgo,[3] Miren Sarasola-Gastesi,[3,5] Leire Escudero-Arrarás,[3] Santiago Milla-Navarro,[6,7] Pedro de la Villa,[6,7] Maialen Sagartzazu-Aizpurua,[8] José Ignacio Miranda,[8] Jesús María Aizpurua,[8] Adolfo López de Munain,[2–4,9] Ainara Vallejo-Illarramendi,[2–4] and Javier Ruiz-Ederra[1,3,5]

[1]Miramoon Pharma, S.L., Donostia-San Sebastian, Spain
[2]Group of Neurosciences, Departments of Pediatrics and Neuroscience, Faculty of Medicine and Nursing, University of Basque Country (UPV/EHU), Donostia-San Sebastian, Spain
[3]Groups of Sensorial Neurodegeneration and Neuromuscular Diseases, Neuroscience Area, Biogipuzkoa Health Research Institute (IIS Biodonostia), Donostia-San Sebastian, Spain
[4]CIBERNED, ISCIII (CIBER, Carlos III Institute, Spanish Ministry of Sciences and Innovation), Madrid, Spain
[5]Department of Dermatology, Ophthalmology and ORL, University of Basque Country (UPV/EHU), Donostia-San Sebastian, Spain
[6]Department of System Biology, University of Alcalá, Alcalá de Henares, Spain
[7]Visual Neurophysiology Group, Instituto Ramon y Cajal de Investigación Sanitaria (IRYCIS), Madrid, Spain
[8]Department of Organic Chemistry-I, Korta Research Center, University of the Basque Country (UPV/EHU), Donostia-San Sebastian, Spain
[9]Department of Neurology, Hospital Universitario Donostia, OSAKIDETZA, Donostia-San Sebastián, Spain

Correspondence: Javier Ruiz Ederra, Department of Dermatology, Ophthalmology and ORL, Faculty of Medicine and Nursing. University of Basque Country (UPV/EHU), Paseo Doctor Begiristain 105, San Sebastian 20014, Spain; javier.ruize@ehu.eus.
Ainara Vallejo Illarramendi, Department of Pediatrics, Faculty of Medicine and Nursing. University of Basque Country (UPV/EHU), Paseo Doctor Begiristain 105, San Sebastian 20014, Spain; ainara.vallejo@ehu.eus.

ALL and KGI contributed equally to this article.

Received: October 15, 2024
Accepted: February 18, 2025
Published: March 26, 2025

Citation: Lara-López A, Gonzalez-Imaz K, Rodríguez-Hidalgo M, et al. Topical administration of novel FKBP12 ligand MP-004 improves retinal function and structure in retinitis pigmentosa models. *Invest Ophthalmol Vis Sci.* 2025;66(3):56. https://doi.org/10.1167/iovs.66.3.56

Purpose. This study evaluates the therapeutic potential of MP-004, a novel FKBP12 ligand, in the treatment of inherited retinal dystrophies (IRDs). MP-004 targets the FKBP12/RyR interaction, which is disrupted in several neurologic disorders with underlying oxidative stress.

Methods. The toxicity and efficacy of MP-004 were examined in vitro in 661W cells. Efficacy was evaluated in phototoxic and H_2O_2-induced damage using impedance assays, calcium imaging, and in situ PLA. In vivo, MP-004 efficacy was evaluated in the *rd10* mouse model of retinitis pigmentosa (RP) by topical ocular instillation. Retinal function was assessed by electroretinography (ERG), visual acuity was measured using a water maze test, and retinal structure was analyzed morphometrically.

Results. MP-004 exhibited low toxicity (LD_{50}: 1.22 mM) and effectively protected 661W cells from phototoxicity (EC_{50}: 30.6 nM). Under oxidative stress conditions, MP-004 preserved the FKBP12.6/RyR2 interaction, restored cytosolic and endoplasmic reticulum calcium levels, and prevented cell death. In vivo, MP-004 significantly preserved retinal function in *rd10* mice, with ERG wave amplitude increases of up to 50% in scotopic and 71% in photopic conditions, corresponding to rod and cone functions, respectively. Additionally, MP-004 improved visual acuity for low spatial frequency patterns and preserved retinal structure, with a 23% increase in outer nuclear layer thickness and preservation in the number of rods and cones and their segment length.

Conclusions. MP-004 shows promise as a therapeutic agent for RP, preserving retinal structure and function, likely through modulation of the FKBP12.6/RyR2 interaction. Further studies are needed to explore its pharmacokinetics and efficacy in other IRD models.

Keywords: IRD, small molecule, eye drop, calcium modulation, ryanodine receptor

Copyright 2025 The Authors

This work is licensed under a Creative Commons Attribution-NonCommercial-NoDerivatives 4.0 International License.

Retinitis pigmentosa (RP) is the most common inherited retinal dystrophy (IRD) and a leading cause of nonpreventable blindness worldwide. Affecting approximately 1 in 4000 people, RP is linked to mutations in over 80 genes, leading to the progressive loss of retinal photoreceptors and irreversible vision loss.[1,2] Despite significant advances in identifying new genes and understanding the molecular mechanisms underlying RP, many aspects of photoreceptor degeneration remain unclear.[3,4] Moreover, like other IRDs, RP currently lacks an effective standardized treatment for most patients.[1,5] Indeed, while gene therapy has shown promise in early-stage IRDs, its application remains limited by the need to target specific mutations or genes.[6] So far, Luxturna (Novartis Europharm Limited, Horsham, UK) is the only product approved for the treatment of Leber congenital amaurosis caused by mutations in the *RPE65* gene, which affects around 1 in 81,000 people.[7]

Photoreceptor death in IRDs, including RP, is driven by multiple pathways, such as the activation of protein kinase G (PKG), calpains, the parthanatos pathway, and apoptosis mediated by caspases and endoplasmic reticulum (ER) stress.[8–11] Many mutations in IRD affect genes related to the phototransduction cascade, frequently causing dysregulation of cGMP, which has been known to be toxic to photoreceptors.[12] High cGMP levels activate PKG and cyclic nucleotide–gated channels (CNGC), increasing intracellular calcium and triggering calcium-activated calpains, especially calpain 1 and calpain 2, with distinct roles in neuroprotection and neurodegeneration, respectively.[12–15] Extensive calpain activation is observed in several RP models, including the *rd1*, *rd2*, and *rd10* mice, as well as other animal models of photoreceptor degeneration.[16]

In the retina, dynamic intracellular calcium fluxes are crucial for visual signal transduction, particularly in photoreceptor outer segments, where cytosolic [Ca^{2+}] is essential for adapting and modulating the phototransduction cascade.[17] Calcium homeostasis is primarily regulated by the CNGC channels and the Na^{+}/Ca^{2+}-K^{+} exchanger (NCK).[18] However, ER and mitochondria also regulate the intracellular concentration of calcium through its release and storage.[19] The main ER channels involved in calcium homeostasis are ryanodine receptors (RyRs) and inositol 1,4,5-trisphosphate receptors (IP3R), which release calcium from the ER lumen into the cytoplasm, and the endo/sarcoplasmic reticulum calcium transporter ATPase (SERCA), which transports calcium back into the ER.[20,21] In pathological conditions, uncontrolled calcium leakage from ER channels may activate cytotoxic pathways in the mitochondria, including reactive oxygen species (ROS) production, autophagy, and apoptosis.[22,23] Three RyR isoforms (RyR1–3) are expressed in the retina.[24] RyR2 has been implicated in photoreceptor death in a mouse model of achromatopsia[25,26] and identified as a key factor in calcium dysregulation and photoreceptor death in CNGC-deficient models. In these models, deletion of RyR2 was found to reduce ER stress and mitigated photoreceptor loss.[25] Additionally, RyR2 overexpression has been linked to worsened photoreceptor degeneration through ER stress and the cGMP pathway.[21]

RyR channels are regulated by a complex system involving various accessory proteins, including FK506 binding proteins FKBP12 and FKBP12.6, which act as molecular switches to ensure proper channel function by stabilizing the closed state of RyR channels, preventing subconductance states, and facilitating coupling between adjacent channels.[27,28] Congenital mutations or posttranslational modifications caused by nitro-oxidative stress may result in dysfunctional leaky RyR channels.[29,30]

Oxidative stress, resulting from the overproduction of ROS, is a significant contributor to photoreceptor cell death in RP, particularly during the secondary cone degeneration that follows rod loss. The role of oxidative stress in photoreceptor death is well documented across various models of retinal degeneration,[31–34] with studies highlighting the protective effects of antioxidants and the role of NADPH oxidase, a key enzyme in ROS production activated by elevated cytosolic calcium levels.[35] Light-induced ROS production has been shown to accelerate retinal degeneration in both inherited and age-related retinopathies, including RP.[31,33]

To address the broader challenge of premature photoreceptor death in IRDs, we have tested the effect of MP-004, a novel FKBP12 ligand, in cellular and animal models of RP. MP-004 belongs to a family of triazole molecules that potentiate FKBP12/RyR interaction and normalize intracellular calcium levels under oxidative stress conditions.[36] In particular, we investigated the hypothesis that MP-004 slows down the progression of photoreceptor cell death in RP models by acting on central pathological mechanisms of photoreceptor degeneration. This hypothesis is grounded on previous works of our group, in which we identified several MP compounds as potential therapeutic candidates to protect myotubes in muscle disorders with underlying nitro-oxidative stress, FKBP12/RyR1 dysfunction, and calcium dysregulation.[36,37] Our strategy aims to modulate a key pathogenic mechanism that is disrupted in most, if not all, IRDs, offering potential benefits regardless of the underlying genetic cause.

Methods

Preparation of MP-004

MP-004, a highly water-soluble salt optimized for ophthalmic applications, was prepared from compound MP-002 (formerly known as AHK2), which was synthesized following a CuAAC "click" methodology from 2-azidoethyl-N,N-dimethylamine and 4-methoxyphenyl propargyl sulfide.[37] To a 0.2 M solution of the resulting 1-[2-[2-[2-(N,N-dimethylamino)ethyl]-4-[(4-methoxyphenyl)thiomethyl]-1*H*-1,2,3-triazole (MP-002) in anhydrous MeOH, cooled to 0 °C, was added 1.0 equiv of chlorotrimethylsilane, and the mixture was stirred for 30 minutes at the same temperature. Evaporation of the solvent under reduced pressure and crystallization from acetone afforded pure nonhygroscopic MP-004 (87%).

Impedance Assays

Impedance was used to evaluate cell cytolysis in efficacy and toxicity assays using 661W mouse photoreceptor cells,[38] kindly provided by Prof. Muayyad Al-Ubaidi (University of Oklahoma). These cells express several cone photoreceptor markers, sharing features of both photoreceptors and retinal ganglion cells, and although they do not fully replicate photoreceptor structure, they are frequently used as an in vitro photoreceptor model.[38–40] In total, 50,000 cells/well were seeded onto extracellular matrix (ECM)-coated CytoView-Z 96-well impedance plates (#Z96-IMP-96B; Axion Biosystems, Atlanta, Georgia, USA) and grown in Dulbecco's modified Eagle's medium (#11594486; Fisher Scientific, Waltham, MA, USA) with 40 µL/L hydrocortisone

21-hemisuccinate sodium salt (#H-2270; Sigma, St. Louis, MO, USA), 40 µL/L progesterone (#P-8783; Sigma), 0.032 g/L putrescine dihydrochloride (#P-7505; Sigma), and 40 µL/L β-mercaptoethanol (#M-6250; Sigma)[41] at 37 °C, 5% CO_2. Experiments were conducted at 90% confluency with cells at passage numbers 25 to 30. Impedance measurements were recorded at 1-minute intervals at 10 kHz using the Maestro Edge system (Axion Biosystems).

Calcium Imaging

Calcium imaging was used to evaluate MP-004 activity in normalizing cytosolic calcium levels in 661W photoreceptor-like cells under oxidative stress. Calcium imaging was performed as previously described[36] using the ratiometric fluorochrome Fura-2 AM (#F1221; ThermoFisher Scientific, Waltham, MA, USA). Briefly, 661W cells were seeded at 3000 cells/well onto ECM-coated µ-Slide 15 Well 3D ibiTreat plates (#AI-81506; Inycom, Zaragoza, Spain) with 1 µM MP-004. After 24 hours, oxidative stress was induced by adding 2 mM H_2O_2 (#349887; Merck, Darmstadt, Germany) for 1 hour. Cells were loaded with 5 µM Fura-2 AM and 2.5 mM ReadiUse probenecid (#20062; Deltaclon, Madrid, Spain) for 30 minutes at 37°C. Calcium imaging was performed at room temperature in imaging buffer (125 mM NaCl, 1.2 mM $MgSO_4$, 5 mM KCl, 25 mM HEPES, 6 mM glucose, 2 mM $CaCl_2$, pH 7.4) using an ECLIPSE Ti-S/L100 microscope (Nikon, Tokyo, Japan) with a 20× S-Fluor objective, a lambda-DG4 illumination system, and an Orca-Flash2.8 camera (Hamamatsu, Bridgewater, NJ, USA) controlled by NisElements software. ER calcium content was estimated by the cytosolic calcium increase induced by 1 µM ionomycin addition in the absence of extracellular calcium. Intracellular calcium concentration was calculated using the ratio of Fura-2 AM fluorescence intensities at 340/380 nm after background correction, applying the following equation: $[Ca^{2+}]i = \beta K_D\ (R - R_{min})/(R_{max} - R)$, with 224 nM as the apparent dissociation constant of Fura-2 AM (K_D).

Ethics Statement and Animal Handling

All animal procedures were conducted following the ARVO Statement for the Use of Animals in Ophthalmic and Vision Research and approved by the Animal Care and Use Committee of Donostia University Hospital and the Clinical Research Ethics Committee of the Basque Country, Spain (CEEA16/013, January 13, 2017). *C57BL6/J* mice (wild-type, WT) were used as controls, and a congenic inbred strain of B6.CXB1-Pde6brd10/J mice in a *C57BL6/J* background (Pde6brd10, *rd10*) was used as a model of RP. Animals were obtained from the Jackson Laboratory (Bar Harbor, ME, USA) and were housed under a 12-hour light/dark cycle at 22 °C with 45% to 55% humidity and free access to food and water at the Biogipuzkoa facility. Mice received daily ocular instillations of 1.5 µL eye drops containing either MP-004 or vehicle (PBS) under inhalation anesthesia. MP-004 was administered for 4 days, from P12 to P15 at 15 µg/eye/d ($n = 36$), to evaluate its effect on protein levels, mRNA expression, and cell viability at an early stage. From P14 to P24, it was administered for 11 days at 15 ($n = 32$) or 30 µg/eye/d ($n = 14$) for immunohistochemical and ERG analyses. Finally, MP-004 was administered for 16 days, from P14 to P29, at 15 µg/eye/day ($n = 9$), for immunohistochemical and visual acuity analyses.

Quantitative Real-Time PCR

Total RNA was extracted using the miRNeasy Mini Kit plus DNaseI (#217084; Qiagen, Hilden, Germany), following the manufacturer's instructions. cDNA was synthesized from 500 ng RNA using the SuperScript Vilo cDNA Synthesis kit (#11754050; Thermo Fisher, Waltham, MA, USA). Quantitative PCR (qPCR) was performed with 10 ng cDNA and analyzed as previously described,[42] using the CFX384 system (Bio-Rad, Hercules, CA, USA), with Power SYBR Green PCR Master Mix (#4367659; Thermo Fisher). Samples were run in technical triplicates, and gene expression was normalized to reference gene *Tbp*. Primer sequences for mRNA validation are shown in Table 1.

Capillary Western Blot

Protein was extracted from WT and *rd10* mouse retinas using RIPA lysis buffer (50 mM Tris-HCl pH 7.2, 0.9% NaCl, 1% NP40, 1 mM EGTA, 1 mM EDTA) containing protease and phosphatase inhibitors (#748443; Thermo Fisher) and inhibitors of calpain I/II and cathepsins B/L (#208719; Sigma). Protein quantification was performed by the Bradford protein assay (#500-0006; Bio-Rad). Capillary Western blot was performed using the Jess instrument (ProteinSimple; Biotechne, Minneapolis, MN, USA), following the manufacturer's instructions. Protein samples were diluted to 0.5 to 2 µg/µL with 5X Fluorescence Master Mix (Biotechne) and denatured at 95 °C for 5 minutes. Samples were loaded onto customary plates (#SM-W004 or #SM-W005; Biotechne) for protein separation. Table 2 shows the list of antibodies used. Chemiluminescence signals were quantified using the Compass software, which generated chemiluminescence spectra and lane view images. Signals were normalized to total protein (#DM-TP01; Biotechne).

Immunohistochemistry

Immunohistochemical characterization was performed in 661W cells and retinal cryosections (7–12 µm) from P16, P25, and P30 mice, as previously described.[43] Briefly, samples were blocked for 1 hour in a solution containing 0.5% Triton X-100, 2% donkey serum, and 2% BSA in PBS and incubated with primary antibodies overnight at 4 °C, followed by a 1-hour incubation of secondary antibodies and DAPI (#D9542; Sigma) at room temperature. Samples were

Table 1. Primer Sequences Used for Quantitative PCR

Gene	Species	Amplicon Size (bp)	Forward Primer	Reverse Primer
CAPN1	Mouse	105	AAACACAAAGACCTGCGCACTA	GAACTCCACCAGACCCAGCTT
CAPN2	Mouse	121	CTTCGGCATCTATGAGGTTCCA	CTCGCGGAGGTTAATGAAGGTAT
CAPN5	Mouse	133	ATTCTGGATGACCT TTGAGGACAT	ATGTCTCGTCCAGGCACCAT
CAPN10	Mouse	148	GGTTCCAGCAGACGGTGAGA	GTAGGTGGAGGGAACAATCCTGTA
iNOS	Mouse	116	CGCTACAACATCCTGGAGGAA	AAACTATGGAGCACAGCCACATT
TBP	Mouse	149	CACAGGAGCCAAGAGTGAAGAA	CCAGCCTTATAGGGAACTTCACAT

Table 2. List of Antibodies Used in Western Blot, Immunohistochemistry, and In Situ PLA Experiments

	Catalog Number	Company	Dilution	Species
PDE6β (B-8)	sc-377486	Santa Cruz Biotechnology	WB 1:50, IF 1:50	Mouse
FKBP12 (1E5-A12)	ab58072	Abcam	WB 1:50, IF 1:50	Mouse
FKBP1B Polyclonal Antibody	PA5109727	Fisher Scientific	WB 1:50	Rabbit
FKBP12.6	AF4174	Biotechne	IF or PLA 1:50	Goat
RyR2	ARR002	Alomone Labs	WB 1:250, IF or PLA 1:100	Rabbit
Activated Calpain 2	ab39165	Abcam	IF 1:100	Rabbit
Rhodopsin (4D2)	MABN15	Sigma	IF 1:500	Mouse
Cone Arrestin	AB15282	Sigma	IF 1:500	Rabbit
Anti-Mouse Secondary HRP	042-205	Biotechne	WB	Goat
Anti-Rabbit Secondary HRP	042-206	Biotechne	WB	Goat
Anti-Goat Secondary HRP	043-522-2	Biotechne	WB	Donkey
Donkey Anti-Mouse IgG (H+L), Alexa Fluor 555	A-31570	Thermo Fisher	IF 1:400	Donkey
Donkey Anti-Goat IgG (H+L), Alexa Fluor 555	A-21432	Thermo Fisher	IF 1:400	Donkey
Donkey Anti-Rabbit IgG (H+L), Alexa Fluor 647	A-31573	Thermo Fisher	IF 1:400	Donkey
Duolink In Situ PLA Probe Anti-Rabbit PLUS	DUO92002	Sigma	PLA 1:5	Donkey
Duolink In Situ PLA Probe Anti-Mouse MINUS	DUO92004	Sigma	PLA 1:5	Donkey
Duolink In Situ PLA Probe Anti-Goat PLUS	DUO92003	Sigma	PLA 1:5	Donkey

HRP, horseradish peroxidase; IF, immunofluorescence; WB, Western blot.

mounted with Prolong Gold Antifade (#P36930; Thermo Fisher) and imaged by confocal microscopy (Zeiss LS900, Oberkochen, Germany). Table 2 shows a list of antibodies used for immunofluorescent (IF) analyses. For analysis, retinal sections were divided into central, mid-peripheral, and peripheral zones, each representing one-third of the total retinal length. At P25, the central zone extended 750 µm from the optic nerve, the mid-peripheral zone spanned 750 to 1500 µm, and the peripheral zone covered 1500 to 2250 µm. For 661W cell analysis, the percentage of $CAPN2^+$ cells was calculated. Four images per well with more than five cells per image were analyzed in five wells per condition.

In Situ Proximity Ligation Assay

Proximity ligation assay (PLA) analysis was used for evaluating FKBP12/RyR2 and FKBP12.6/RyR2 interaction in 661W cells or retinal cryosections as previously described.[36,37] For cellular assays, 661W cells were seeded onto µ-Slide 15 Well 3D Glass Bottom (#81507; Ibidi, Gräfelfing, Germany) at 3000 cells/well. Then, 1 µM MP-004 treatment was added at seeding, and after 24 hours, oxidative stress was induced by adding 2 mM H_2O_2 for 1 hour. Cells and retinal cryosections (7 µm) were incubated overnight at 4 °C with RyR and FKBP12/12.6 antibodies (Table 2). The Duolink in situ PLA Far red assay kit (#DUO92013; Sigma) was used with corresponding conjugated probes (#DUO92002, #DUO92004, #DUO92003; Sigma, described in Table 2). Samples were mounted with ProLong Gold antifade reagent with DAPI (#P36962; Life Technologies, Eugene, OR, USA) and imaged with a Zeiss LS900 confocal microscope. Images were processed and analyzed using the ImageJ software (National Institutes of Health, Bethesda, MD, USA) based on previous studies.[44,45] For retinal sections, local background in PLA images was removed in ImageJ by processing each image with a median filter followed by a watershed technique to obtain individual dots, and particles between 0.1 and 10 µm^2 were analyzed. For these samples, colocalization was analyzed in the outer nuclear layer (ONL) and photoreceptor segments (outer segment [OS]/inner segment [IS]), and for each localization, data are represented as coverage (percentage of area of PLA signal/total area). At least 15 images per mouse were analyzed. In cells, particles between 0.1 and 10 µm^2 were directly analyzed. The number of particles in each image was quantified and normalized to the number of nuclei. At least 30 images per condition were analyzed with an average of three cells per image.

TUNEL Assay

The TUNEL assay was used to evaluate photoreceptor cell death in retinal sections, as previously described.[43] Retinal cryosections (7 µm) from P14 and P16 mice were evaluated using the DeadEnd Fluorometric TUNEL System (# G3250; Promega, Madison, WI, USA), following the manufacturer's instructions. Slides were mounted with DAPI-containing medium for nuclear visualization and analyzed by confocal fluorescence microscopy (Zeiss LS900). The free ImageJ macro, TUNEL Cell Counter, was used for image analysis.[46]

Electroretinogram Recordings

Full-field ERG was used to evaluate retinal function in P25 *rd10* mice. Animals were treated with MP-004 (15 or 30 µg/eye/d) from P14 to P24, and untreated littermates were used as controls. ERG protocols followed International Society for Clinical Electrophysiology of Vision guidelines and were performed as previously described[47] with minor modifications. After overnight dark adaptation, anesthetized mice were placed on a 37 °C heating pad, and mydriasis was induced with 1% tropicamide. Full-field flash ERG responses were recorded using a custom-made Ganzfeld stimulator, with increasing light flash intensities (−3 to 1 log cd·s/m^2). Rod and cone mixed responses (b-mixed) were recorded under scotopic conditions. Responses were averaged, with intervals between flashes of 1.2 to 15 seconds. Cone responses (b-wave, photopic) were recorded after 5 minutes of light adaptation using 30 cd/m^2 background white light, with a 1.2-second interval between flashes. Scotopic and photopic responses were amplified using an NL104A preamplifier and NL100AK amplifier (Digitimer LTD, Hertfordshire, UK) and filtered using a bandpass filter set between 0.3 and 1000 Hz. All records were digitized using a PowerLab 4/30 (Adinstruments, Oxfordshire, UK).

Investigative Ophthalmology & Visual Science

Visual Acuity Based on Water Maze

Visual acuity was assessed to evaluate visual function in P30 mice using a water maze, as previously described.[48] *Rd10* animals were treated daily for 16 days, from P14 to P29, with 15 µg MP-004/eye/d. The test was conducted in a square tank (70 × 40 cm) filled with water (24–26 °C), opaque on all sides except the front, where a screen was placed (Supplementary Fig. S1). The screen was vertically divided into two equal parts: half displayed a pattern of moving vertical bars, while the other half remained blank. The direction of the bars was randomized, with 50% moving to the right and 50% to the left, and the speed remained constant throughout the procedure. Mice were acclimated to the experimental conditions for 1 week before testing, learning to associate the area of the screen with the moving bars with the location of a submerged, hidden platform placed adjacent to that screen area. This platform, invisible under dim lighting, allowed the mice to escape from the water. During training, a high-contrast bar pattern (100%) with an optimal spatial frequency (0.088 cycles/degree) was used. In the experiment, the contrast and spatial frequency parameters were progressively adjusted until the mice could no longer detect the bar pattern.[49] Contrast sensitivity was determined by calculating the inverse of the minimum contrast at which the mice achieved a hit rate greater than 50%.

Data Analysis

Data are expressed as mean or median ± SD, unless otherwise specified. The sample size for each experiment was calculated using G-power software (Franz Faul, University of Kiel, Germany), with a statistical power of 80% and an alpha error of 0.05. Statistical analysis was performed using GraphPad Prism 8.3.0 (GraphPad Software, La Jolla, CA, USA) and RStudio (Boston, MA, USA).[50,51] Normality was assessed using the Shapiro–Wilk test and Q–Q plots. Normally distributed data were analyzed using *t*-tests or ANOVA followed by appropriate post hoc tests. For nonnormal data, the Kruskal–Wallis test with Dunn's post hoc test was applied. A hierarchical mixed-effects model was used for statistical analyses when a significant improvement in model fit was observed, as previously reported.[52] Pairwise comparisons were adjusted using the Bonferroni correction for multiple testing. In all cases, P values <0.05 were considered statistically significant.

Results

MP-004 Presents a Low Toxicity Profile and High Efficacy in Protecting 661W Photoreceptor-Like Cells From Phototoxicity

In vitro toxicity and efficacy of MP-004 were evaluated in 661W photoreceptor-like cells using impedance

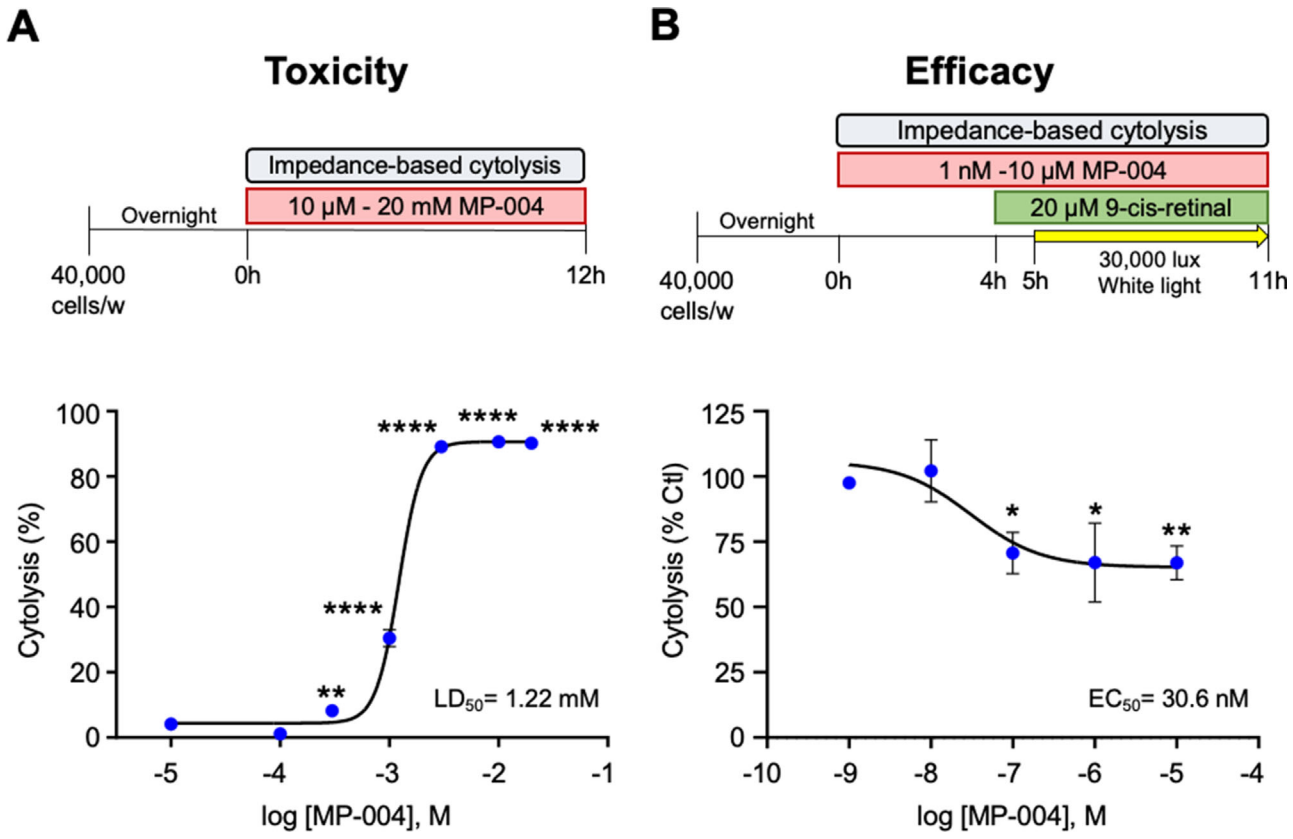

Figure 1. MP-004 *in vitro* toxicity and efficacy in 661W cells. (**A**) *Upper*: Schematic representation of the MP-004 toxicity assay. *Lower*: MP-004 toxicity dose–response curve. LD_{50}, MP-004 median lethal dose after 12 hours. Data are expressed as mean ± SEM, $n = 4$ wells. $^{\#}{}^{*}P < 0.01$, $^{****}P < 0.0001$, one-way ANOVA with Dunnett's post hoc test versus nontreated. (**B**) *Upper*: Schematic representation of the phototoxicity assay used to determine MP-004 efficacy. *Lower*: Efficacy curve of MP-004 in a light-induced photoreceptor cell death model induced by 9-*cis*-retinal (20 µM) and white light (30,000 lux). MP-004 effect was measured after 6 hours, and data are expressed as cytolysis percentage versus nontreated. EC_{50}, half maximal effective concentration of MP-004. Data are expressed as mean ± SEM from $N = 3$ independent experiments performed in three to six replicates. $^{*}P < 0.05$, $^{**}P < 0.01$, two-way ANOVA with Dunnett's post hoc test versus nontreated.

Investigative Ophthalmology & Visual Science

measurements. For toxicity dose–response curves, cells were exposed for 12 hours to seven doses of MP-004 ranging from 10 µM to 20 mM. MP-004 showed low toxicity, with an in vitro median lethal dose (LD_{50}) of 1.22 mM (Fig. 1A).

To analyze the in vitro efficacy of MP-004, we used a previously reported phototoxicity assay in which 9-*cis*-retinal and high-intensity white light were used to induce photoreceptor death due to conversion of 9-*cis*-retinal to all-*trans*-retinal.[53,54] In 661W cells, we found that after 6 hours of exposure, 20 µM 9-*cis*-retinal and 30,000 lux white light caused 45% cytolysis, while MP-004 protected 661W cells against 9-*cis*-retinal and light-induced phototoxicity in a dose–response manner with a half-maximal effective concentration (EC_{50}) of 30.6 nM (Fig. 1B). The maximum effect was achieved at a 100-nM concentration of MP-004 and resulted in around 30% protection of phototoxicity ($P = 0.017$). The in vitro therapeutic index of MP-004 derived from the toxicity (LD_{50}) and efficacy (EC_{50}) data was 40,000, which indicates a wide therapeutic window and a minimal risk of toxicity at therapeutic doses.

MP-004 Protects From Calcium Dysregulation and 661W Photoreceptor-Like Cell Death Induced by Oxidative Stress

MP-004 compound has previously shown activity in human myotubes under nitro-oxidative stress as a calcium normalizer by stabilizing the FKBP12/RyR1 interaction.[37] Since oxidative stress is a major contributor to photoreceptor degeneration in RP,[10] we first wanted to evaluate the activity of MP-004 in rescuing photoreceptor cell death and calcium dysregulation induced by oxidative stress. To this end, we used H_2O_2 to induce oxidative stress in the 661W photoreceptor cell line. First, we assessed the median lethal dose (LD_{50}) of H_2O_2 by performing life impedance measurements on 661W cells treated with 0 to 10 mM H_2O_2 for 3 hours. We found that the LD_{50} of H_2O_2 was 2 mM (Supplementary Fig. S2), and thus, this concentration was used to induce oxidative stress in 661W cells in subsequent experiments.

Next, we evaluated whether MP-004 was effective in reducing H_2O_2-induced toxicity in 661W cells (Figs. 2A–D). Indeed, Fig. 2B shows a representative H_2O_2 cytolysis curve measured by impedance assays. Pretreatment of 661W cells under oxidative stress with 1 µM MP-004 for 2 days resulted in a significantly reduced cytolysis over time compared to nontreated cells ($P = 0.0056$, Fig. 2B). In fact, MP-004 significantly reduced cell cytolysis from 50% in H_2O_2-treated cells to 23.5% in H_2O_2 + MP-004, representing an overall cell death reduction of 53% ($P < 0.0001$, Fig. 2C). Furthermore, while nontreated cells took 2.7 hours on average to reach 50% death, or kill time 50 (KT_{50}), MP-004–treated cells took a significantly longer time with a KT_{50} of 3.8 hours, representing a 35% increase in KT_{50} ($P < 0.0001$, Fig. 2D).

We next sought to evaluate whether MP-004 was able to normalize cytosolic calcium levels in H_2O_2-treated 661W cells by performing calcium live-cell imaging with Fura2-AM ratiometric fluorochrome (Figs. 3A–C). Our data showed that 1 hour after addition of 2 mM H_2O_2, cytosolic calcium levels were significantly increased by 10-fold in 661W cells under oxidative stress compared to control cells ($P < 0.001$). Moreover, pretreatment with MP-004 for 2 days significantly reduced this cytosolic calcium elevation by 24% ($P = 0.01216$, Fig. 3B). Next, we determined whether increased cytosolic calcium levels observed in photoreceptors under oxidative stress were associated with reduced calcium content in the ER (Fig. 3C). Interestingly, we found that under oxidative stress, ER calcium content in H_2O_2-treated cells was drastically reduced 2.7-fold ($P < 0.01$), which suggests that in 661W photoreceptor-like cells, oxidative stress induces calcium depletion from ER stores. Most importantly, pretreatment with MP-004 was able to fully restore ER calcium content in oxidative stressed cells to basal levels ($P = 0.0012$, Fig. 3C).

Given that our results are consistent with leaky RyR channels as potential mediators of oxidative stress–induced photoreceptor death, we next decided to evaluate whether FKBP12/RyR interaction was altered in 661W photoreceptor-like cells under oxidative stress. RyR2 is reported to be

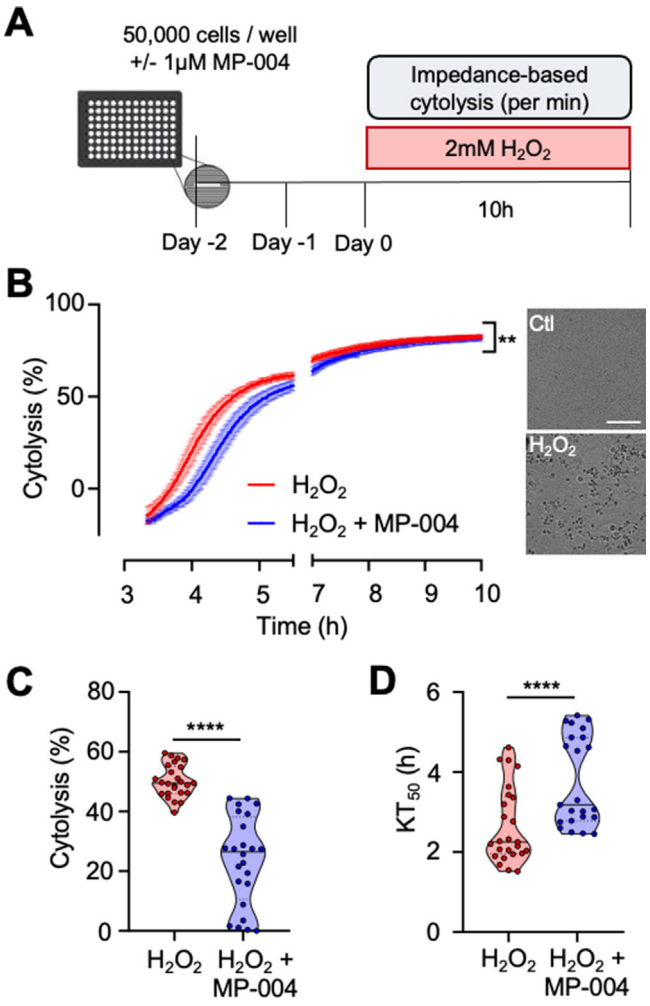

Figure 2. MP-004 prevents oxidative stress toxicity in 661W photoreceptor-like cells. (**A**) Schematic representation of impedance-based cytolysis assay. (**B**) Representative cytolysis time curves induced by 2 mM H_2O_2. *Red* shows nontreated cells, and *blue* shows cells treated with 1 µM MP-004. Data are expressed as mean ± SEM, $n = 5$ wells/group. $^{**}P < 0.01$, Kolmogorov–Smirnov test between curves. *Right*: Brightfield images from cultures 6 hours after H_2O_2 addition. *Scale bar*: 100 µm. (**C**) MP-004 protection against H_2O_2-induced cytolysis was evaluated at the point of 50% cytolysis in nontreated cells and (**D**) KT_{50}, kill-time 50. *Dots* represent individual wells ($n = 49$) from five independent experiments. $^{****}P < 0.0001$, hierarchical mixed effects with pairwise comparisons and Bonferroni correction for multiple testing.

Investigative Ophthalmology & Visual Science

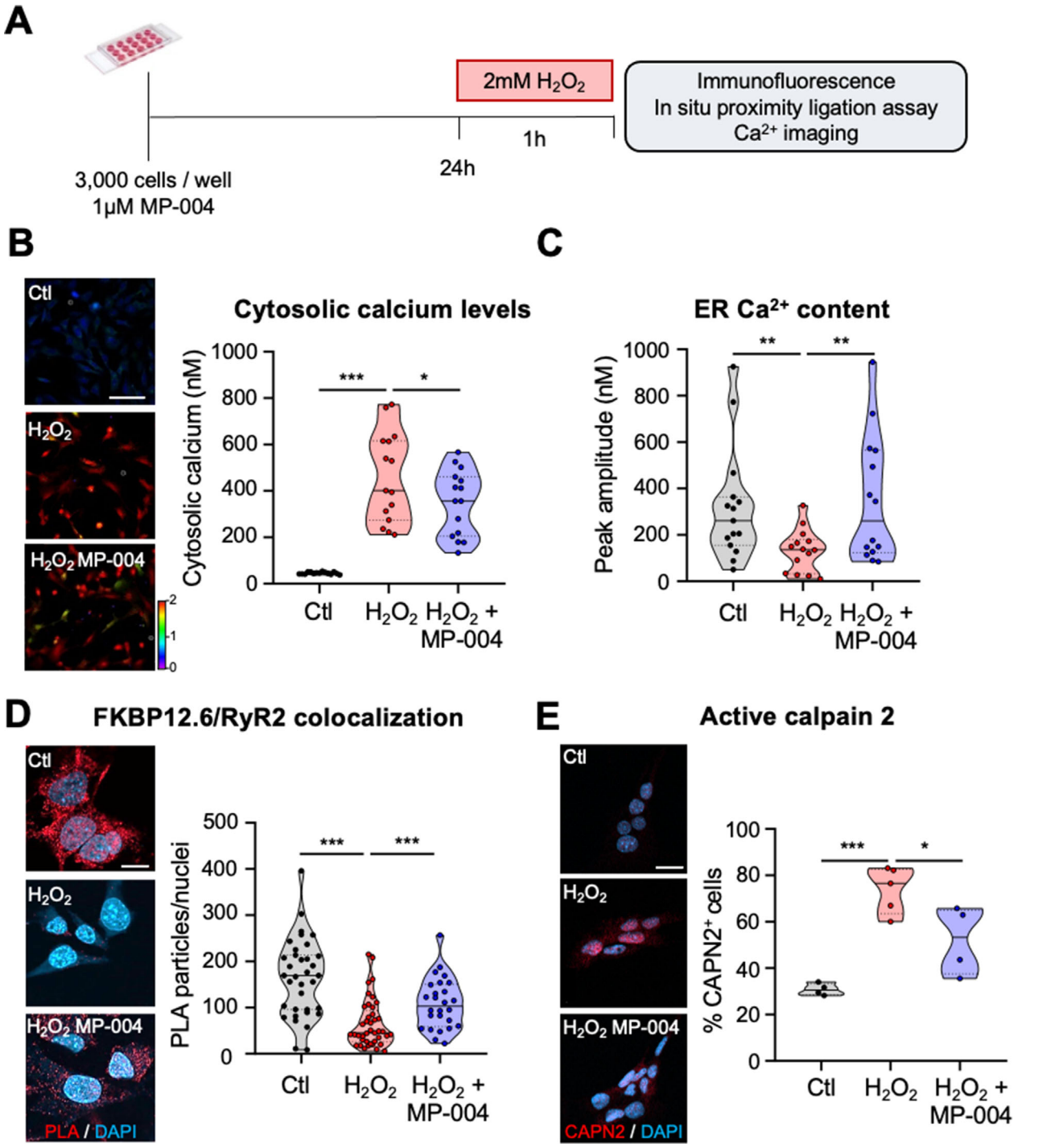

Figure 3. MP-004 restores intracellular calcium homeostasis and FKBP12.6/RyR2 interaction, preventing CAPN2 expression in H_2O_2-treated 661W cells. (**A**) Schematic representation of the experimental protocol. (**B**) Cytosolic calcium levels and (**C**) ER calcium content 1 hour after the addition of 2 mM H_2O_2. *Dots* represent values from individual wells ($n = 45$ wells). *$P < 0.05$, ***$P < 0.001$, hierarchical mixed effects with pairwise comparisons and Bonferroni correction for multiple testing. *Left*: Representative pseudocolored images showing basal Fura-2 AM 340/380 ratios. *Scale bar*: 200 µm. (**D**) FKBP12.6/RyR2 colocalization by in situ PLA. *Left*: Representative images. PLA signal (*red*); nuclei (DAPI, *blue*). *Scale bar*: 10 µm. *Right*: PLA signal quantification presented as violin plots with the median and interquartile range. *Dots* represent the number of particles per nucleus ($n = 102$ images from two independent experiments). ***$P < 0.001$, hierarchical mixed-effects model with pairwise comparisons and Bonferroni correction for multiple testing. (**E**) Percentage of active calpain 2–positive cells after oxidative stress. $CAPN2^+$ signal (*red*); nuclei (DAPI, *blue*). Scale bar: 30 µm. *Right*: Quantification of CAPN cells presented as violin plots with the median and interquartile range ($n = 5$ independent wells, with each well representing the mean of four images). *$P < 0.05$, ***$P < 0.001$, one-way ANOVA with Dunnett's post hoc test versus H_2O_2.

Investigative Ophthalmology & Visual Science

the major isoform expressed in retina[24] and has previously been implicated in photoreceptor degeneration.[25,26] In the heart, it is generally accepted that RyR2 is stabilized mainly by FKBP12.6 protein and that the loss of FKBP12.6/RyR2 interaction results in leaky RyR2 channels.[29,55,56] Therefore, we next wanted to evaluate FKBP12.6/RyR2 interaction in 661W cells under oxidative stress. To do this, we used the in situ PLA technique, which has been extensively used by our group and others to evaluate protein–protein interaction,[57–59] including FKBP12 with RyRs.[36,37] Our results show that upon H_2O_2 exposure, photoreceptors sustain a 60% loss of FKBP12.6/RyR2 interaction ($P < 0.0001$, Fig. 3D). Remarkably, this effect occurs 1 hour after addition of H_2O_2, well before the onset of cell death, and therefore, it constitutes an early event within the oxidative stress cascade. Interestingly, pretreatment with MP-004 successfully prevented the loss of the FKBP12.6/RyR2 interaction, as evidenced by a significant increase in their colocalization up to 66% ($P < 0.001$, Fig. 3D). Next, we aimed to investigate CAPN2 activation in response to H_2O_2-induced oxidative stress in 661W cells. One hour after H_2O_2 treatment, the percentage of $CAPN2^+$ cells was significantly increased around 3-fold in H_2O_2-treated cells ($P = 0.0002$), as shown in Figure 3E. Furthermore, pretreatment with MP-004 led to a significant 30% reduction in the $CAPN2^+$ activation in H_2O_2-treated cells ($P = 0.0194$). Overall, our results indicate that MP-004 protects 661W photoreceptor-like cells from oxidative stress death by stabilizing the FKBP12.6/RyR2 interaction and normalizing ER calcium dysregulation and calpain 2 activation.

Disruption of FKBP12/RyR2 Interaction in the Retina of *rd10* Mice

The expression and distribution of RyR2 and FKBP12 proteins have not been studied in the *rd10* mouse model, so we aimed to investigate these proteins in WT and *rd10* mouse retinas during the process of photoreceptor degeneration. Western blot analysis was performed to assess the expression levels of retinal proteins in WT and *rd10* mice at P12, P14, P16, and P25 (Supplementary Fig. S3A). As expected, PDE6B, which is mutated in *rd10* mice, showed significant differences between WT and *rd10* samples, with a significant 60% to 80% reduction in the protein levels observed from P12 throughout the period analyzed. In contrast, no significant differences in protein levels were observed for RyR2, FKBP12, and FKBP12.6 between WT and *rd10* retinas. Likewise, immunohistochemistry studies (Fig. 4A) showed no differences in protein distribution for FKBP12, FKBP12.6, and RyR2 between WT and *rd10* at P16 or at P14 (Supplementary Fig. S4). These proteins are primarily localized in the OS/IS of photoreceptors, with additional expression observed in the ONL (Fig. 4A). To further investigate FKPB12/RyR2 protein interaction, we performed an in situ PLA in P14 and P16 WT and *rd10* mouse retinas. At P14, our analysis revealed a significant reduction in the ONL of FKBP12.6/RyR2 and FKBP12/RyR2 colocalization by 33% and 54%, respectively (Fig. 4B). FKBP12.6/RyR2 colocalization showed mean values of 6.43 ± 1.78 (WT) and 4.32 ± 2.02 (*rd10*, $P = 0.03$), and FKBP12/RyR2 showed mean values of 6.2 ± 2.45 (WT) and 2.87 ± 0.98 (*rd10*, $P = 0.013$). Furthermore, FKBP12.6/RyR2-decreased interaction persisted at P16 in the photoreceptor segments (16.55 ± 2.94 in WT vs. 11.5 ± 3.89 in *rd10*, $P = 0.04$). Overall, our results indicate an early disruption of RyR2 interaction with FKBP12 and FKBP12.6 in the *rd10* mouse photoreceptors, before the onset of photoreceptor cell death.

MP-004 Reduces iNOS Expression and Early Photoreceptor Cell Death in *rd10* Mice

To investigate the efficacy of MP-004 in vivo, we first assessed its biodistribution to determine if topical administration via ocular instillation could deliver therapeutically relevant concentrations to the retina. The data collected 48 hours after a subsequent dose of 18 µg MP-004 were analyzed. MP-004 was administered to the WT mouse in 3-µL PBS eye drops, and MP-004 concentration was measured in the retina by HPLC–mass spectrometry over a 48-hour period (Supplementary Fig. S5). Within the first 24 hours, the compound achieved retinal concentrations ranging from 0.5 to 1.5 µg/g, corresponding to an average concentration of 3.5 µM, which exceeds the effective concentration previously observed in vitro. Our data also indicate that subsequent doses maintain a consistent threshold concentration in the retina, above 2 µg/g (or 6.8 µM), fluctuating between 1 and 5.3 µg/g, with an average concentration of 3 µg/g.

Once confirmed that MP-004 reached the retina, we proceeded to study its effects on photoreceptor degeneration during the early stages of the disease. To this end, we treated *rd10* mice by ocular instillation with 15 µg/eye/d MP-004 from P12 to P15, and retinas were analyzed at P16 (Fig. 5A). First, we verified that MP-004 had no significant impact on the protein levels of PDE6B, RyR2, FKBP12, and FKBP12.6 (Supplementary Fig. S3B). Then, we examined the expression of calpains, a family of proteins largely implicated in photoreceptor degeneration in IRDs and other retinal disorders.[12] mRNA analysis revealed moderate increases of 20% to 30% in *CAPN1*, *CAPN2*, and *CAPN5* expression in *rd10* retinas, with *CAPN2* showing a significant 35% increase in *rd10* retinas compared to WT ($P = 0.011$, Bonferroni). Treatment with MP-004 seemed to decrease *CAPN2* overexpression, although no statistical significance was achieved (Fig. 5B).

Next, we aimed to investigate whether MP-004 could reduce oxidative stress–induced retinal damage in vivo, using inducible nitric oxide synthase (iNOS), a maker of oxidative stress, since iNOS upregulation leads to large quantities of nitric oxide and peroxynitrite formation, contributing to cellular damage. Our analysis revealed a 72% increase in *iNOS* mRNA levels in P16 *rd10* retinas compared to WT ($P < 0.0001$), which was significantly reduced by 71% with a 4-day MP-004 pretreatment compared to untreated *rd10* retinas ($P = 0.0153$, Fig. 5C).

Given that calpain 2 activity has been identified as a key event during rod photoreceptor cell death in the *rd10* model,[13] we conducted an immunohistochemical analysis to evaluate the influence of MP-004 on calpain 2 activation in *rd10* mice at P16. Similar to previous results at P18,[13] P16 *rd10* mice displayed a drastic elevation of active calpain 2 in the photoreceptor cells, with median numbers of activated calpain 2–positive cells in the ONL of 35 ± 20 cells/mm^2 for WT, 1577 ± 257 cells/mm^2 for *rd10*, and 854 ± 1299 cells/mm^2 for *rd10* mice (Fig. 5D). At P16, active calpain 2 distribution was restricted to the central retina, consistent with the characteristic central-to-peripheral degeneration gradient observed in this model.[13,43] Notably, neither

Investigative Ophthalmology & Visual Science

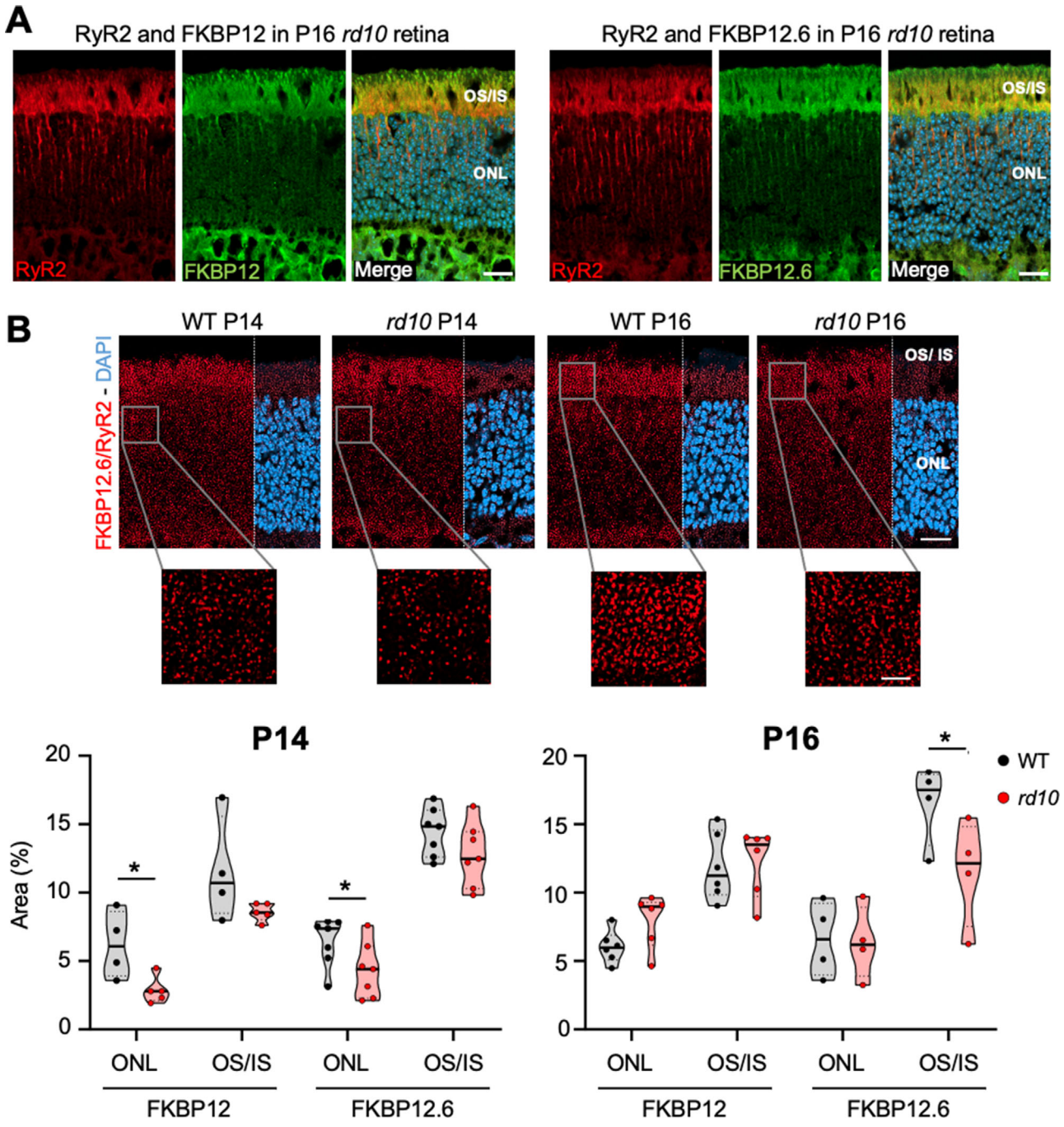

Figure 4. Characterization of RyR2, FKBP12, and FKBP12.6 in the mouse retina. (**A**) Representative immunofluorescent images of P16 *rd10* retina sections. RyR2 (*red*), FKBP12 (*green*, *left*), FKBP12.6 (*green*, *right*), nuclei (*blue*). *Scale bar*: 20 µm. (**B**) In situ PLA analysis showing colocalization of FKBP12/RyR2 and FKBP12.6/RyR2 in retinas from WT and *rd10* mice at P14 and P16. *Lower*: High-magnification insets. *Scale bar*: 5 µm. PLA (*red*), nuclei (*blue*). *Scale bar*: 20 µm. *Lower*: The quantification of PLA signals in the ONL and photoreceptor OS/IS. *Dots* represent mean values from individual mice. At least 15 images were taken per retina. *$P < 0.05$, one-tail unpaired *t*-test.

the increase in calpain 2 activation in *rd10* retinas nor the 46% protection of MP-004 reached statistical significance, likely due to the high variability observed at the P16 stage.

We then assessed photoreceptor cell death using the TUNEL assay at postnatal days 14 and 16 (P14 and P16), before the onset of degeneration and at an early stage of degeneration, respectively. At P14, both WT and *rd10* retinas exhibited low levels of TUNEL-positive cells in the photoreceptor layer, with means of 24 ± 14 and 34 ± 27 cells/mm^2, respectively (Fig. 6A). By P16, however, *rd10* mice showed a marked increase in TUNEL-positive cells, averaging 9742 ± 5410 cells/mm^2, compared to 206 ± 197 cells/mm^2 in WT mice, indicating significant photoreceptor loss ($P < 0.0001$, Fig. 6B). At P16, TUNEL and calpain 2–positive cells showed a similar distribution with a predominant localization in the central retina. However, some TUNEL-positive cells were also observed in mid-peripheral regions. MP-004

Investigative Ophthalmology & Visual Science

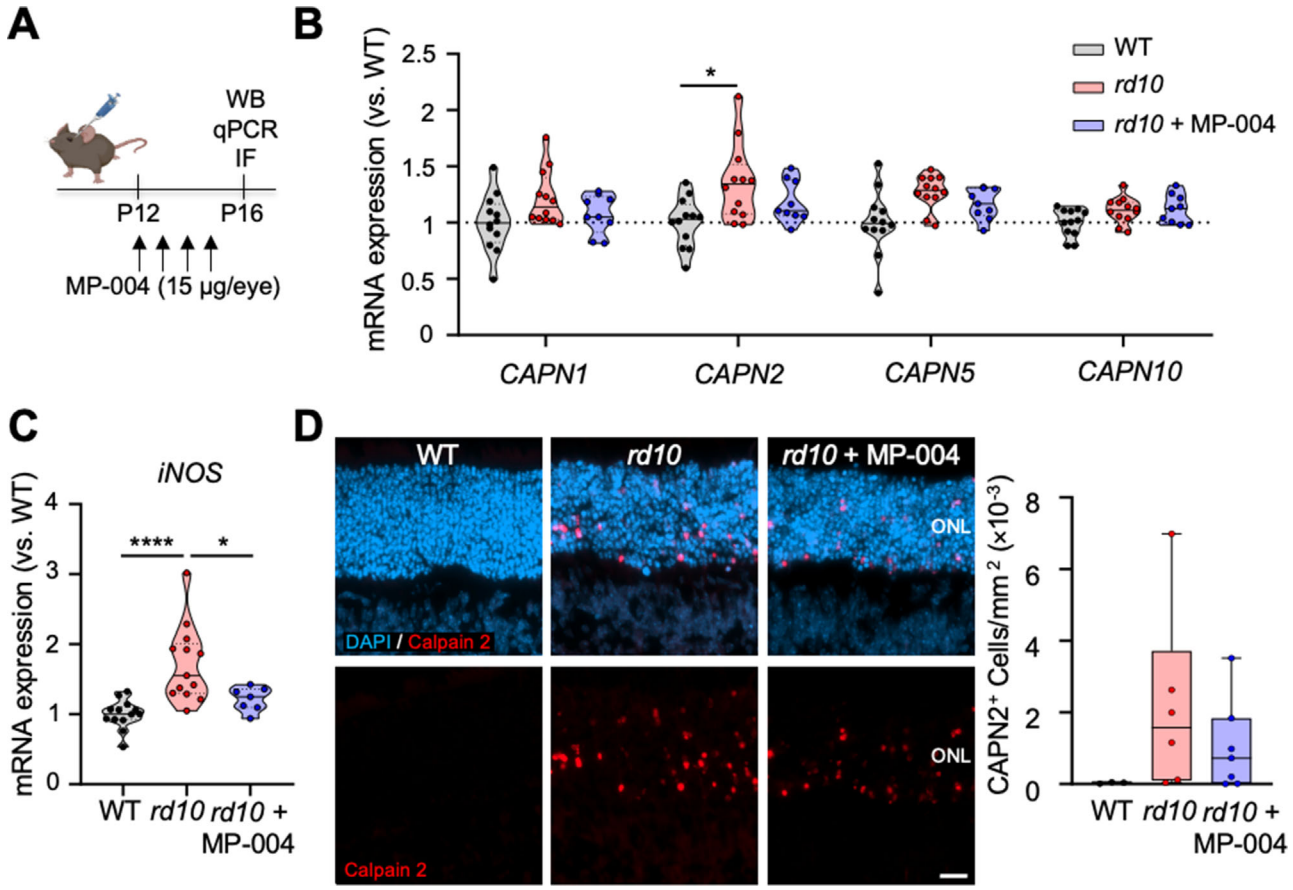

Figure 5. Effect of MP-004 on calpains and iNOS expression in P16 *rd10* mice. (**A**) Schematic representation of the treatment regimen used for subsequent assays. (**B**) mRNA expression levels of calpains in the mouse retina. *rd10* mice were treated daily with either vehicle or MP-004 (15 µg/eye) via topical administration from P12 to P15. Data are expressed as the mean fold change relative to WT levels. *Dots* represent individual retinas ($n = 33$ retinas). *$P < 0.05$, hierarchical mixed-effects model with pairwise comparisons and Bonferroni correction for multiple testing. (**C**) iNOS mRNA expression levels in the mouse retina. *rd10* mice were treated daily with either vehicle or MP-004 (15 µg/eye) via topical administration from P12 to P15. Data are expressed as the mean fold change relative to WT levels. *$P < 0.05$, ****$P < 0.0001$, one-way ANOVA with Tukey's post hoc test. (**D**) Immunohistochemical analysis of active calpain 2 in the *rd10* mouse retina at P16. *Left*: Representative immunofluorescent images of WT and *rd10* retinal sections. *Right*: Quantification of the number of calpain 2–positive cells per millimeter squared. Data are displayed as violin plots with the median and interquartile range. *Dots* represent values from individual mice. Kruskal–Wallis analysis showed no statistical significance among the three groups. *Scale bar*: 20 µm.

treatment provided a 56% protection against photoreceptor cell death in *rd10* retinas by reducing the number of TUNEL-positive cells to 4421 ± 7127 cells/mm^2 ($P = 0.0006$), which demonstrates its neuroprotective effect in the retina (Fig. 6B).

MP-004 Enhances ERG Response, Visual Acuity, and Retinal Structure in *rd10* Mice

This study aimed to evaluate the effects of MP-004 on visual function in *rd10* mice during postnatal days 25 to 30 (P25–P30), a stage characterized by advanced photoreceptor degeneration.[60–63] Starting at P14, the mice received daily ocular instillations of MP-004 at 15 µg per eye for 11 days (Figs. 7A–D) or 16 days (Figs. 7E–H).

ERG was conducted at P25 to assess rod and cone function under scotopic and photopic conditions, respectively. The b-wave response was used as an indirect measurement of photoreceptor activity. The mixed response representing the combined activity of both rod and cone photoreceptors (downward deflection), followed by a b-wave (upward deflection), indicates bipolar cell activity postsynaptic to the photoreceptors.[64]

As previously reported,[65] *rd10* mice exhibited a marked reduction in the amplitudes of mixed a/b-waves under scotopic conditions. However, MP-004 treatment led to a significant increase in b-wave amplitudes under mixed and photopic conditions compared to vehicle-treated *rd10* mice (Figs. 7B–D). Specifically, ERG analysis revealed significant improvements in b-wave amplitudes in the retinas of MP-004–treated *rd10* mice. Under mixed conditions, b-wave amplitude increased by 50% ($P = 0.0125$), 44% ($P = 0.0003$), and 30% ($P = 0.0002$) at stimulus intensities of 0.35, 0.67, and 1 log cd·s/m^2, respectively, with daily MP-004 treatment of 15 µg per eye (Fig. 7C). Under photopic conditions, a 71% increase in b-wave amplitude was observed at −0.5 log cd·s/m^2 ($P = 0.0007$), suggesting that MP-004 improves both rod and cone function (Fig. 7D). Additionally, treatment with 15 µg MP-004 significantly reduced a-wave mixed implicit times at stimulus intensities from −0.043 to 0.796 log cd·s/m^2 (Supplementary Fig. S6).

Investigative Ophthalmology & Visual Science

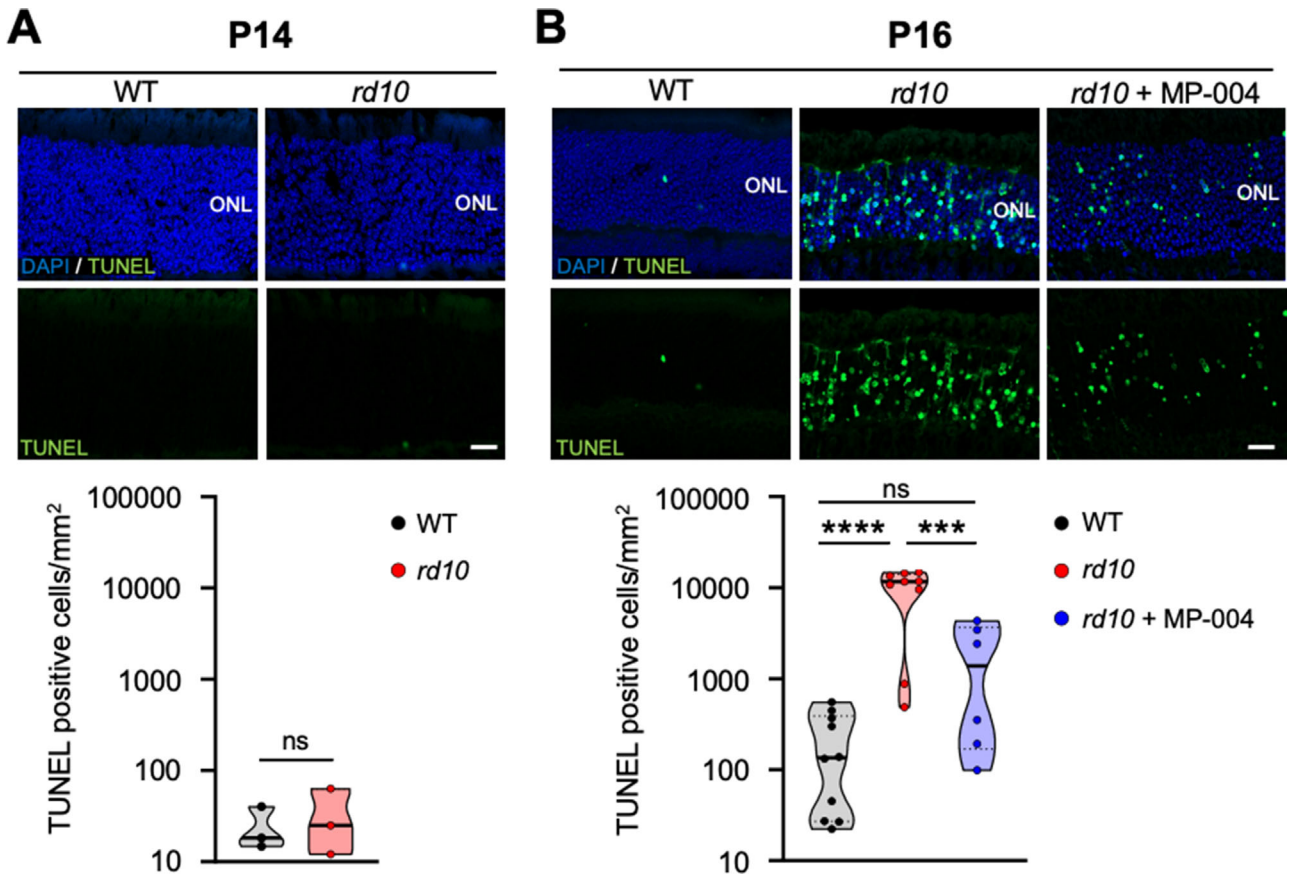

Figure 6. MP-004 reduces photoreceptor death in P16 *rd10* mice. (**A**) Analysis of cell death in P14 WT and *rd10* mice. *Upper*: Representative images of TUNEL staining (*green*) and DAPI (*blue*). *Scale bar*: 20 µm. *Lower*: Quantification of TUNEL-positive cells per millimeter squared. No significant differences were observed between WT and *rd10* mice at P14 (one-tailed unpaired *t*-test; NS, nonsignificant). (**B**) Analysis of cell death in P16 *rd10* mice treated with vehicle or MP-004 (15 µg/eye) for 4 days. *Upper*: Representative images of TUNEL staining (*green*) and DAPI (*blue*). Scale bar: 20 µm. *Lower*: Quantification of TUNEL-positive cells per millimeter squared. Data are displayed as violin plots with the median and interquartile range. *Dots* represent values from individual mice. ***$P < 0.001$, ****$P < 0.0001$, one-way ANOVA with Tukey's post hoc test.

To further determine whether the improvements in retinal function translated into enhanced visual acuity, a modified water maze test was performed at P30, allowing for the required training period for the animals (Fig. 7F). Contrast sensitivity was measured across a range of spatial frequencies (0.011–0.355 cycles/degree). A trend toward improved visual acuity was observed in MP-004–treated animals, with statistically significant differences at the lowest spatial frequency (0.011 cycles/degree, $P < 0.05$), which represents one of the most challenging conditions. This suggests an improvement in low-contrast visual capacity.

Retinal morphometric analysis of P30 *rd10* mice revealed that MP-004 treatment led to a 56% increase in mid-peripheral ONL retinal thickness ($P = 0.0012$, Figs. 7G, 7H) and an improved preservation of retinal structure as determined by rhodopsin and cone arrestin immunofluorescence (Fig. 7H). Altogether, this indicates a protective effect of MP-004 on retinal structure. However, at P25, no significant differences were observed between MP-004–treated *rd10* mice and untreated littermates in terms of the ONL thickness or the number of photoreceptors (Supplementary Fig. S7). Despite this, P25 *rd10* mice treated with MP-004 demonstrated significant improvements in rod and cone activity, as evidenced by our ERG results.

To further assess the efficacy of MP-004 on the preservation of retinal cytoarchitecture, we evaluated the effects of MP-004 at a higher dosage of 30 µg/eye/d (Fig. 8A). At the functional level, ERG analysis revealed similar effects of MP-004 to those observed in *rd10* mice treated with the lower dose of 15 µg/eye/d (Figs. 8B, 8C). Specifically, ERG data demonstrated a significant increase in b-wave amplitude of 33% ($P = 0.018$), 42% ($P = 0.0006$), and 37% ($P < 0.0001$) at 0.35, 0.67, and 1 log cd·s/m^2, respectively, under mixed lighting conditions (Fig. 8C).

More importantly, treatment of *rd10* mice with 30 µg/eye/d resulted in significant structural preservation of the retinal cytoarchitecture by P25. Morphometric analysis revealed a 24% increase in ONL thickness in the central retina ($P = 0.0103$) and a 23% increase in the mid-peripheral retina ($P = 0.0285$) (Figs. 8D, 8E). Furthermore, the number of rods was markedly preserved, with a 61% increase in rod cells in the central retina ($P < 0.0001$) and a 76% increase in the peripheral retina ($P = 0.0048$). Cone cell numbers also showed an increase of 28% in the central retina ($P = 0.0001$). Moreover, MP-004 treatment at 30 µg/eye/d effectively preserved photoreceptor segment length, with a 33% increase in the central retina ($P = 0.0198$) and a 64% increase in the periphery ($P = 0.0078$).

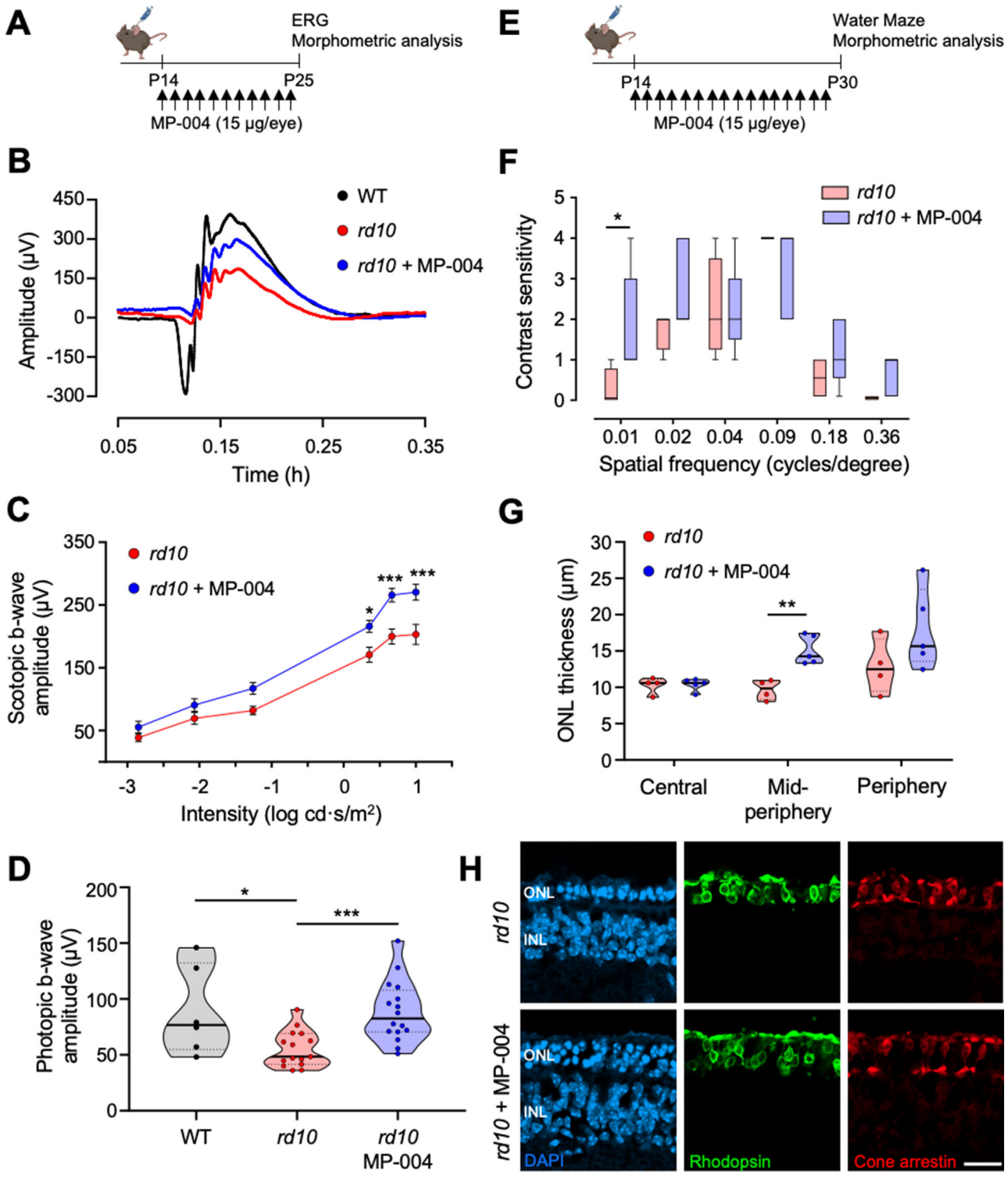

Figure 7. In vivo efficacy of MP-004 in *rd10* mice at a daily dose of 15 µg per eye. (**A**) Schematic representation of the treatment regimen. *rd10* mice received daily ocular instillations (1.5 µL per eye) of 15 µg/eye MP-004 or PBS vehicle from P14 to P24 and were sacrificed at P25 following ERG recordings. (**B**) Representative ERG recordings from P25 WT (*black*) and *rd10* mice treated with either MP-004 (*blue*) or vehicle (PBS, *red*) from P14 to P24. (**C**) Intensity-response curves of mixed b-waves (scotopic) to light stimuli (−3 to 1 log cd × s/m^2) in *rd10* mice treated with MP-004 or vehicle. Data are expressed as mean ± SEM (n = 38 mice). *P < 0.05, ***P < 0.001, two-way ANOVA followed by Sidak's post hoc test. (**D**) Amplitude of cone responses (b-wave, photopic) to light stimuli (−0.5 log cd × s/m^2) in WT and *rd10* mice treated with MP-004 or vehicle (n = 37 mice). *P < 0.05, ***P < 0.001, Kruskal–Wallis test. (**E**) Schematic representation of the extended treatment regimen. *rd10* mice received daily ocular instillations (1.5 µL per eye) of 15 µg/eye MP-004 or PBS vehicle from P14 to P29 and were sacrificed at P30 following the water maze test. (**F**) Efficacy of MP-004 on visual acuity in P30 *rd10* mice. Data are presented as box-and-whisker plots showing the median and interquartile range (n = 9 mice). *P < 0.05, Mann–Whitney test. (**G**) Quantification of ONL thickness in P30 *rd10* retinal sections. *Dots* represent values from individual mice. Data are displayed as violin plots showing the median and interquartile range. **P < 0.01, one-tailed unpaired t-test. (**H**) Representative immunofluorescent images of P30 *rd10* retinal sections showing nuclei (DAPI, *blue*), rhodopsin (*green*), and cone arrestin (*red*) distribution. *Scale bar*: 20 µm.

Investigative Ophthalmology & Visual Science

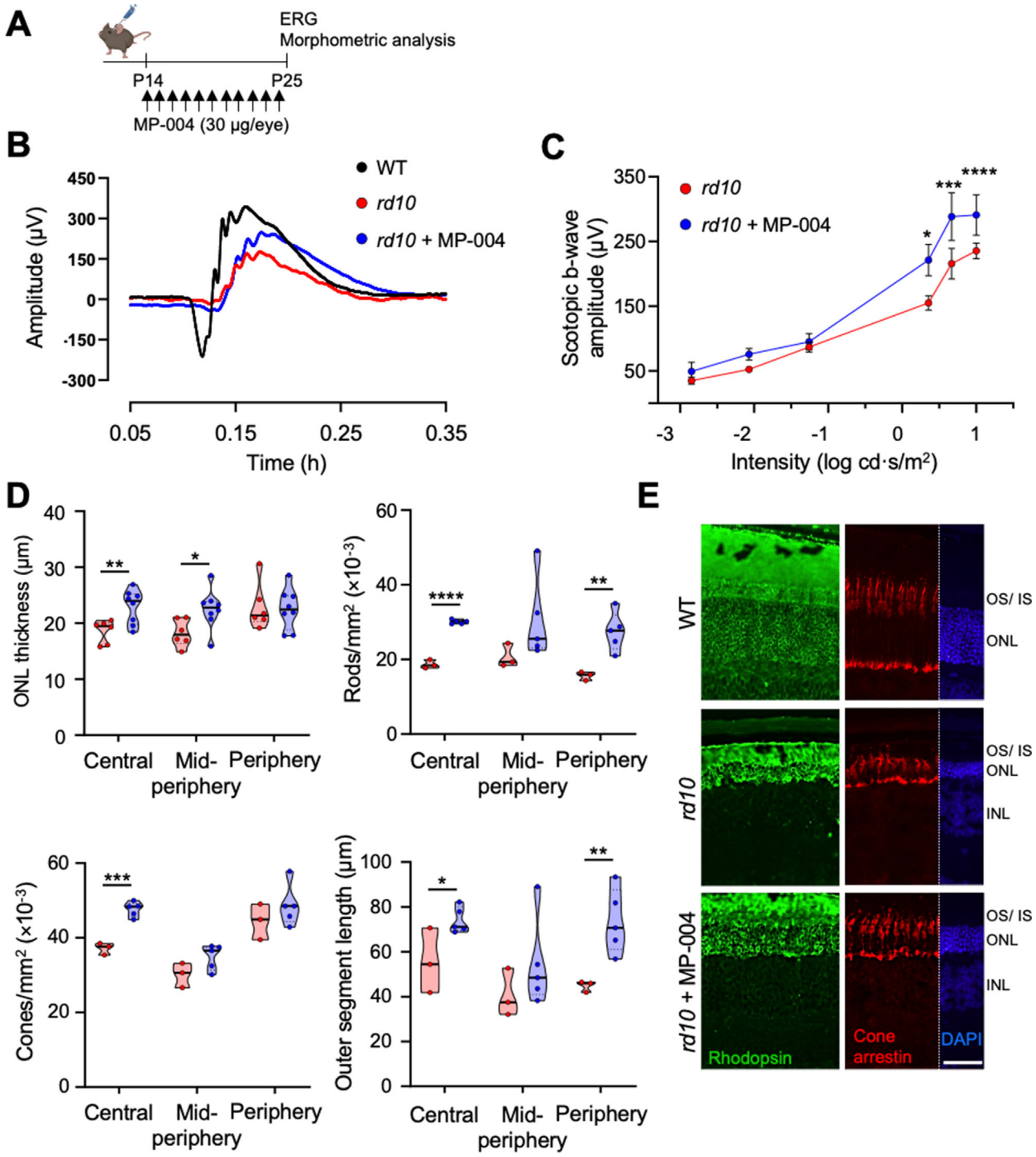

Figure 8. In vivo efficacy of MP-004 in *rd10* mice at a daily dose of 30 µg per eye. (**A**) Schematic representation of the treatment regimen. *rd10* mice received daily ocular instillations (1.5 µL per eye) of 30 µg/eye MP-004 or PBS vehicle from P14 to P24 and were sacrificed at P25 following ERG recordings. (**B**) Representative ERG recordings from P25 WT (*black*) and *rd10* mice treated with MP-004 (*blue*) or vehicle (*red*) from P14 to P24. (**C**) Intensity-response curves of ERG b-waves to light stimuli (−3 to 1 log cd × s/m^2) in *rd10* mice treated with MP-004 or vehicle. Data are expressed as mean ± SEM (n = 14 mice). *P < 0.05, ***P < 0.001, ****P < 0.0001, two-way ANOVA followed by Sidak's post hoc test. (**D**) Morphometric analysis of P25 *rd10* retinas, including ONL thickness, number of rods and cones per millimeter squared, and photoreceptor outer segment length. Data are presented as violin plots showing the median and interquartile range. *Dots* represent values from individual mice. *P < 0.05, **P < 0.01, ***P < 0.001, ****P < 0.0001, one-tailed unpaired t-test. (**E**) Representative immunofluorescence images of P25 central retinal sections from WT, untreated *rd10*, and MP-004–treated *rd10* mice. Staining includes nuclei (DAPI, *blue*), rhodopsin (*green*), and cone arrestin (*red*). INL, inner nuclear layer. *Scale bar*: 20 µm.

Investigative Ophthalmology & Visual Science

These findings underscore the dose-dependent efficacy of MP-004, demonstrating substantial functional and structural benefits at higher doses.

Discussion

This study presents a novel therapeutic approach for RP using MP-004, a new FKBP12 ligand known to stabilize FKBP12/RyR interaction and normalize calcium levels under nitro-oxidative stress.[36,37] In cellular models of oxidative stress, MP-004 significantly enhanced RyR2 and FKBP12.6 interaction, restoring ER calcium levels and preventing photoreceptor death under stress conditions. Additionally, in the *rd10* mouse model of RP, topical administration of MP-004 reduced photoreceptor death and preserved visual function and retinal architecture during the early stages of degeneration. These findings support MP-004 as a promising therapeutic candidate for RP and other IRDs and support our working hypothesis that MP-004 reduces photoreceptor degeneration likely by preventing calpain 2 activation.

In RP, oxidative stress is a major contributor to photoreceptor degeneration.[10,31,32] This oxidative stress can initiate a vicious cycle in which elevated ROS levels generate leaky RyR channels, which impact mitochondria and further increase ROS production, ultimately leading to cell degeneration.[66] In 661W cells, we have shown that oxidative stress induces early calcium dysregulation, characterized by increased cytosolic calcium levels and depleted ER calcium stores. A previous study in 661W cells reported that sustained cGMP elevation leads to high intracellular calcium levels, ROS generation, and calpain activation,[12,14,15,67] suggesting a close interrelationship between calcium dysregulation and oxidative stress in IRDs.

Excessive calcium release from the ER is a well-documented trigger of photoreceptor death, largely due to mitochondrial dysfunction and activation of the parthanatos pathway and calpains.[8,11] In this study, we show that MP-004 significantly reduces cell death, reduces elevated cytosolic calcium levels, and replenishes ER calcium stores in oxidative-stressed 661W cells, suggesting that MP-004 has a protective role against H_2O_2-induced damage in photoreceptor cells. MP-004 activity on elevated cytosolic calcium concentration of stressed 661W cells is less remarkable than its effect on ER calcium content. This could be attributed to the high concentration of H_2O_2 used (2 mM) and the fact that ROS affect not only RyR channels but also multiple calcium regulatory components such as Ca^{2+} transport at the plasma membrane, store-operated calcium entry, voltage-gated calcium channels, and SERCA and IP3 receptors in the ER.[68] In any case, the restoration of depleted ER calcium stores by MP-004 indicates that RyR2 contributes to ER calcium depletion driven by oxidative stress.

In 661W cells, we found that oxidative stress disrupts the interaction between FKBP12.6 and RyR2, while MP-004 significantly preserves this interaction. These findings are consistent with our previous studies where MP compounds effectively restored the FKBP12/RyR1 interaction and calcium homeostasis in human myotubes subjected to nitro-oxidative stress.[36,37] Interestingly, we found that the interaction between RyR2 and FKBP12/12.6 is compromised in the *rd10* mouse model at P14, well before major neurodegeneration occurs, hitting at an early role for RyR2 and impaired ER calcium signaling in RP. Other studies have linked RyR2 dysfunction to photoreceptor degeneration in IRDs,[25,26] reinforcing the hypothesis that disrupted ER calcium signaling is a common pathological mechanism in these diseases. These findings indicate that MP-004 could be beneficial in RyR2-mediated calcium dysregulation in RP and possibly across a spectrum of IRDs.

Light-induced photoreceptor damage has been linked to mutations in genes associated with the visual cycle, phototransduction, and retinal health, such as *Rhodopsin*, *Abca4*, *Cralpb*, *Crb1*, *Eys*, *Mertk*, *peripherin/Rds*, *Rdh12*, and genes involved in melanin production.[69–74] Phototoxicity significantly contributes to retinal degeneration through mechanisms that involve excessive ROS production and calcium dysregulation, ultimately leading to photoreceptor death and vision loss.[75,76] In RP, the interplay of oxidative stress and light exposure is particularly detrimental, accelerating the degeneration of cone cells following the loss of rod photoreceptors.[10,77] Several studies have shown that rearing *rd10* mice in darkness delays photoreceptor degeneration by up to 2 months.[78] Our findings in 661W cells demonstrate that MP-004 has a protective effect against light-induced phototoxicity with an effective concentration of 30.6 nM, highlighting its therapeutic potential for IRDs and other retinal diseases where light-induced damage is well documented, such as age-related macular degeneration and diabetic retinopathy.[79,80]

Our in vitro findings were confirmed in the *rd10* mouse model of RP, where MP-004 was administered daily via ocular instillation. A short 4-day treatment with MP-004 led to a 55% reduction in photoreceptor cell death, suggesting that MP-004 enhances photoreceptor survival by inhibiting calcium-mediated cell death. While calpain 2 activation is involved in calcium-induced cell death in *rd10* mice,[8,81] the high variability observed in P16 *rd10* mice limited definitive conclusions about its role in MP-004 photoreceptor protection. Notably, calpain 2 activation accounted for less than 20% of TUNEL-positive cells, and its distribution was restricted to the central retina at P16, whereas TUNEL-positive cells were also present in the mid-peripheral retina, suggesting the involvement of other key players in early photoreceptor death in *rd10* mice. Future experiments will focus on studying the other cell death pathways to further elucidate the MP-004 effect on photoreceptor protection. Additionally, a more detailed analysis of MP-004 retinal delivery and potential side effects on other ocular structures should be conducted, addressing the correlation between in vitro toxic doses and retinal concentrations, which remains to be experimentally validated. On the other hand, given the chronic nature of RP and other IRDs, a sustained treatment strategy may be necessary to prevent ongoing photoreceptor cell death. Future studies will be crucial in assessing the long-term efficacy of MP-004 and its potential limitations as a therapeutic intervention for retinal degeneration, particularly regarding the duration of its protective effects.

The preservation of photoreceptors through topical MP-004 resulted in improved retinal function, as evidenced by ERG analysis that showed increased b-wave amplitudes, particularly in bipolar rod pathways, which are primarily affected in RP.[65] These functional improvements, along with enhanced visual acuity, indicate that MP-004 activity extends beyond cellular protection, translating into meaningful physiological benefits. MP-004 treatment, particularly at a higher dosage, preserved the retinal architecture, which is crucial for sustaining visual function in RP in the long term.

MP-004 represents a promising advancement in the treatment of RP by selectively modulating the FKBP12/RyR2

Investigative Ophthalmology & Visual Science

interaction during oxidative stress. This targeted approach effectively addresses calcium dysregulation compared to conventional calcium channel blockers like diltiazem, which may lead to further calcium depletion and adversely affect photoreceptor survival.[82] Several therapeutic strategies for RP are currently being explored, including the administration of neurotrophic factors via an adeno-associated viral vector,[83] GSK-3 modulators,[84] and cGMP analogues that inhibit PKG.[85,86] While these strategies show potential, they are not without risks, as they may negatively impact phototransduction or carry additional risks associated with chronic systemic administration.[85] Ultimately, the future of RP treatment likely lies in combined therapies that simultaneously target multiple pathways to effectively combat this complex disease.

In conclusion, MP-004 represents a promising new approach for the treatment of RP, as it directly addresses calcium dysregulation and oxidative stress, two of the key drivers of photoreceptor degeneration in this disease. MP-004 demonstrates efficacy in preserving photoreceptor integrity in the *rd10* mouse model and in a photoreceptor-like cell line subjected to high oxidative stress or phototoxicity. This, in combination with its noninvasive topical administration, positions MP-004 as a promising therapeutic candidate not only for RP and IRDs but also for more common ophthalmic diseases such as diabetic retinopathy or age-related macular degeneration. Further exploration of MP-004, particularly its biodistribution in larger animal models and its efficacy in other models of retinopathy, would significantly broaden its impact, potentially transforming the therapeutic landscape for both RP and other eye diseases with underlying oxidative stress and calcium dysregulation.

Acknowledgments

The authors thank Mª Carmen Sampedro from Servicio Central de Análisis Unidad de Álava, SGIker at UPV/EHU, and Laura Ramirez from the University of Alcalá for their excellent technical support. The authors also thank Carlo Manno from Rush University Medical Center, Chicago, IL, and Maider Mateo-Abad from the Methodological Support Unit at IIS Biogipuzkoa for their expertise and assistance in statistical analysis and Virginia Arechavala for kindly reviewing the final version of the manuscript. Part of the immunohistochemistry and PLA images were acquired on the confocal microscope in Dr. Jacobo Paredes's laboratory at Tecnun, San Sebastian. ChatGPT and DeepL Write were solely used for assisting in English correction and clarity of the manuscript.

Supported by MCIU/AEI/10.13039/501100011033 and European Union NextGenerationEU/PRTR (CPP2022-009867, JR-E; PID2020-119780RB-I00, AV-I; DIN2020-011302, AL-L); Gobierno Vasco (MTVD24/BG/003 and MTVD23/BD/008, JR-E; IT1732-22, AV-I; IT1741-22, JMA and MS-A; and Pre-2019-1-0325, MR-H); Diputación Foral de Gipuzkoa (2023-CIEN-000032-01, JR-E); and grants from the BEGISARE Foundation and Susana Monsma Foundation (JR-E).

Disclosure: **A. Lara-López**, Miramoon Pharma (E); **K. Gonzalez-Imaz**, None; **M. Rodríguez-Hidalgo**, None; **M. Sarasola-Gastesi**, None; **L. Escudero-Arrarás**, None; **S. Milla-Navarro**, None; **P. de la Villa**, None; **M. Sagartzazu-Aizpurua**, None; **J.I. Miranda**, Miramoon Pharma (O); **J.M. Aizpurua**, Miramoon Pharma (O); **A. López de Munain**, Miramoon Pharma (O); **A. Vallejo-Illarramendi**, Miramoon Pharma (O); **J. Ruiz-Ederra**, Miramoon Pharma (O)

References

1. Verbakel SK, van Huet RAC, Boon CJF, et al. Non-syndromic retinitis pigmentosa. *Prog Retin Eye Res*. 2018;66:157–186.
2. O'Neal TB, Luther EE. *Retinitis Pigmentosa*. Treasure Island, FL: StatPearls Publishing; 2024, http://www.ncbi.nlm.nih.gov/pubmed/29597005. Accessed May 24, 2024.
3. Broadgate S, Yu J, Downes SM, Halford S. Unravelling the genetics of inherited retinal dystrophies: past, present and future. *Prog Retin Eye Res*. 2017;59:53–96.
4. Mustafi D, Arbabi A, Ameri H, Palczewski K. Retinal gene distribution and functionality implicated in inherited retinal degenerations can reveal disease-relevant pathways for pharmacologic intervention. *Pharmaceuticals*. 2019;12(2):74.
5. Hanany M, Rivolta C, Sharon D. Worldwide carrier frequency and genetic prevalence of autosomal recessive inherited retinal diseases. *Proc Natl Acad Sci USA*. 2020;117(5):2710–2716.
6. Sahni JN, Angi M, Irigoyen C, et al. Therapeutic challenges to retinitis pigmentosa: from neuroprotection to gene therapy. *Curr Genomics*. 2011;12(4):276–284.
7. Maguire AM, Simonelli F, Pierce EA, et al. Safety and efficacy of gene transfer for Leber's congenital amaurosis. *N Engl J Med*. 2008;358(21):2240–2248.
8. Li S, Ma H, Yang F, Ding X. cGMP signaling in photoreceptor degeneration. *Int J Mol Sci*. 2023;24(13):11200.
9. Olivares-González L, Velasco S, Campillo I, Rodrigo R. Retinal inflammation, cell death and inherited retinal dystrophies. *Int J Mol Sci*. 2021;22(4):1–19.
10. Newton F, Megaw R. Mechanisms of photoreceptor death in retinitis pigmentosa. *Genes (Basel)*. 2020;11(10):1–29.
11. Yan J, Chen Y, Zhu Y, Paquet-Durand F. Programmed non-apoptotic cell death in hereditary retinal degeneration: crosstalk between cGMP-dependent pathways and parthanatos? *Int J Mol Sci*. 2021;22(19):10567.
12. Das S, Chen Y, Yan J, et al. The role of cGMP-signalling and calcium-signalling in photoreceptor cell death: perspectives for therapy development. *Pflugers Arch Eur J Physiol*. 2021;473(9):1411–1421.
13. Power MJ, Rogerson LE, Schubert T, Berens P, Euler T, Paquet-Durand F. Systematic spatiotemporal mapping reveals divergent cell death pathways in three mouse models of hereditary retinal degeneration. *J Comp Neurol*. 2020;528(7):1113–1139.
14. Goll DE, Thompson VF, Li H, Wei W, Cong J. The calpain system. *Physiol Rev*. 2003;83(3):731–801.
15. Baudry M. Calpain-1 and calpain-2 in the Brain: Dr. Jekill and Mr Hyde? *Curr Neuropharmacol*. 2019;17(9):823–829.
16. Arango-Gonzalez B, Trifunović D, Sahaboglu A, et al. Identification of a common non-apoptotic cell death mechanism in hereditary retinal degeneration. *PLoS One*. 2014;9(11):e112142.
17. Sakurai K, Vinberg F, Wang T, Chen J, Kefalov VJ. The $Na^+/Ca2^+$, K^+ exchanger 2 modulates mammalian cone phototransduction. *Sci Rep*. 2016;6(1):1–10.
18. Baehr W, Palczewski K, eds. *Photoreceptors and Calcium*. Vol 514. Boston, MA, US: Springer; 2002.
19. Krizaj D, Copenhagen DR. Calcium regulation in photoreceptors. *Front Biosci*. 2002;7:d2023–d2044.
20. Križaj D. Calcium stores in vertebrate photoreceptors. *Adv Exp Med Biol*. 2012;740:873–889.
21. Yang F, Ma H, Butler MR, Ding XQ. Potential contribution of ryanodine receptor 2 upregulation to cGMP/PKG signaling-induced cone degeneration in cyclic nucleotide-gated channel deficiency. *FASEB J*. 2020;34(5):6335–6350.

22. Marchi S, Patergnani S, Missiroli S, et al. Mitochondrial and endoplasmic reticulum calcium homeostasis and cell death. *Cell Calcium*. 2018;69:62–72.
23. Shinde V, Kotla P, Strang C, Gorbatyuk M. Unfolded protein response-induced dysregulation of calcium homeostasis promotes retinal degeneration in rat models of autosomal dominant retinitis pigmentosa. *Cell Death Dis*. 2016;7(2):e2085–e2085.
24. Shoshan-Barmatz V, Zakar M, Shmuelivich F, Nahon E, Vardi N. Retina expresses a novel variant of the ryanodine receptor. *Eur J Neurosci*. 2007;26(11):3113–3125.
25. Ma H, Yang F, Butler MR, Rapp J, Le YZ, Ding XQ. Ryanodine receptor 2 contributes to impaired protein localization in cyclic nucleotide-gated channel deficiency. *eNeuro*. 2019;6(3):ENEURO.0119-19.2019.
26. Yang P, Lockard R, Titus H, et al. Suppression of cGMP-dependent photoreceptor cytotoxicity with mycophenolate is neuroprotective in murine models of retinitis pigmentosa. *Invest Ophthalmol Vis Sci*. 2020;61(10):25.
27. Gong D, Yan N, Ledford HA. Structural basis for the modulation of ryanodine receptors. *Trends Biochem Sci*. 2021;46(6):489–501.
28. Hadiatullah H, He Z, Yuchi Z. Structural insight into ryanodine receptor channelopathies. *Front Pharmacol*. 2022; 13:897494.
29. Fernández-Morales JC, Xia Y, Renzo TJ, Zhang XH, Morad M. Mutation in RyR2-FKBP Binding site alters $Ca2^{+}$ signaling modestly but increases "arrhythmogenesis" in human stem cells derived cardiomyocytes. *Cell Calcium*. 2022; 101:102500.
30. Dridi H, Liu Y, Reiken S, et al. Heart failure-induced cognitive dysfunction is mediated by intracellular Ca2+ leak through ryanodine receptor type 2. *Nat Neurosci*. 2023;26(8):1365–1378.
31. Wang J, Li M, Geng Z, et al. Role of oxidative stress in retinal disease and the early intervention strategies: a review. *Oxid Med Cell Longev*. 2022;2022:7836828.
32. Murakami Y, Nakabeppu Y, Sonoda K-H. Oxidative stress and microglial response in retinitis pigmentosa. *Int J Mol Sci*. 2020;21(19):7170.
33. Kushwah N, Bora K, Maurya M, Pavlovich MC, Chen J. Oxidative stress and antioxidants in age-related macular degeneration. *Antioxidants*. 2023;12(7):1379.
34. Zhang SM, Fan B, Li YL, Zuo ZY, Li GY. Oxidative stress-involved mitophagy of retinal pigment epithelium and retinal degenerative diseases. *Cell Mol Neurobiol*. 2023;43(7):3265–3276.
35. Haruta M, Bush RA, Kjellstrom S, et al. Depleting Rac1 in mouse rod photoreceptors protects them from photo-oxidative stress without affecting their structure or function. *Proc Natl Acad Sci USA*. 2009;106(23):9397–9402.
36. Aizpurua JM, Miranda JI, Irastorza A, et al. Discovery of a novel family of FKBP12 "reshapers" and their use as calcium modulators in skeletal muscle under nitro-oxidative stress. *Eur J Med Chem*. 2021;213:113160.
37. Passannante R, Gómez-Vallejo V, Sagartzazu-Aizpurua M, et al. Pharmacokinetic evaluation of new drugs using a multi-labelling approach and pet imaging: application to a drug candidate with potential application in neuromuscular disorders. *Biomedicines*. 2023;11(2):253.
38. Tan E, Ding XQ, Saadi A, Agarwal N, Naash MI, Al-Ubaidi MR. Expression of cone-photoreceptor-specific antigens in a cell line derived from retinal tumors in transgenic mice. *Invest Ophthalmol Vis Sci*. 2004;45(3):764–768.
39. Wheway G, Nazlamova L, Turner D, Cross S. 661W photoreceptor cell line as a cell model for studying retinal ciliopathies. *Front Genet*. 2019;10(APR):421628.
40. Sayyad Z, Sirohi K, Radha V, Swarup G. 661W is a retinal ganglion precursor-like cell line in which glaucoma-associated optineurin mutants induce cell death selectively. *Sci Rep*. 2017;7(1):16855.
41. Al-Ubaidi MR, Matsumoto H, Kurono S, Singh A. Proteomics profiling of the cone photoreceptor cell line, 661W. *Adv Exp Med Biol*. 2008:613:301–311.
42. Lasa-Elgarresta J, Mosqueira-Martín L, González-Imaz K, et al. Targeting the ubiquitin-proteasome system in limb-girdle muscular dystrophy with CAPN3 mutations. *Front Cell Dev Biol*. 2022;10:822563.
43. Anasagasti A, Ezquerra-Inchausti M, Barandika O, et al. Expression profiling analysis reveals key microRNA-mRNA interactions in early retinal degeneration in retinitis pigmentosa. *Invest Ophthalmol Vis Sci*. 2018;59(6):2381–2392.
44. George J, Mittal S, Kadamberi IP, Pradeep S, Chaluvally-Raghavan P. Optimized proximity ligation assay (PLA) for detection of RNA-protein complex interactions in cell lines. *STAR Protoc*. 2022;3(2):101340.
45. Hegazy M, Cohen-Barak E, Koetsier JL, et al. Proximity ligation assay for detecting protein-protein interactions and protein modifications in cells and tissues in situ. *Curr Protoc cell Biol*. 2020;89(1):e115.
46. Maidana DE, Tsoka P, Tian B, et al. A novel ImageJ macro for automated cell death quantitation in the retina. *Invest Ophthalmol Vis Sci*. 2015;56(11):6701–6708.
47. Corrochano S, Barhoum R, Boya P, et al. Attenuation of vision loss and delay in apoptosis of photoreceptors induced by proinsulin in a mouse model of retinitis pigmentosa. *Invest Ophthalmol Vis Sci*. 2008;49(9):4188–4194.
48. Prusky GT, West PWR, Douglas RM. Behavioral assessment of visual acuity in mice and rats. *Vis Res*. 2000;40(16):2201–2209.
49. Cha S, Ahn J, Jeong Y, et al. Stage-dependent changes of visual function and electrical response of the retina in the rd10 mouse model. *Front Cell Neurosci*. 2022;16:926096.
50. Kuznetsova A, Brockhoff PB, Christensen RHB. lmerTest package: tests in linear mixed effects models. *J Stat Softw*. 2017;82(13):1–26.
51. Bates D, Mächler M, Bolker BM, Walker SC. Fitting linear mixed-effects models using lme4. *J Stat Softw*. 2015;67(1):1–48.
52. Sikkel MB, Francis DP, Howard J, et al. Hierarchical statistical techniques are necessary to draw reliable conclusions from analysis of isolated cardiomyocyte studies. *Cardiovasc Res*. 2017;113(14):1743–1752.
53. Chen Y, Okano K, Maeda T, et al. Mechanism of all-trans-retinal toxicity with implications for Stargardt disease and age-related macular degeneration. *J Biol Chem*. 2012;287(7):5059–5069.
54. Kanan Y, Moiseyev G, Agarwal N, Ma JX, Al-Ubaidi MR. Light induces programmed cell death by activating multiple independent proteases in a cone photoreceptor cell line. *Invest Ophthalmol Vis Sci*. 2007;48(1):40–51.
55. Fauconnier J, Thireau J, Reiken S, et al. Leaky RyR2 trigger ventricular arrhythmias in Duchenne muscular dystrophy. *Proc Natl Acad Sci USA*. 2010;107(4):1559–1564.
56. Richardson SJ, Thekkedam CG, Casarotto MG, Beard NA, Dulhunty AF. FKBP12 binds to the cardiac ryanodine receptor with negative cooperativity: implications for heart muscle physiology in health and disease. *Philos Trans R Soc B Biol Sci*. 2023;378(1879):20220169.
57. Alam MS. Proximity ligation assay (PLA). *Curr Protoc Immunol*. 2018;123(1):e58.
58. Wang P, Yang Y, Hong T, Zhu G. Proximity ligation assay: an ultrasensitive method for protein quantification and its applications in pathogen detection. *Appl Microbiol Biotechnol*. 2021;105(3):923–935.
59. Young RM. Proximity ligation assay. *Methods Mol Biol*. 2019;1956:363–370.

Investigative Ophthalmology & Visual Science

60. Barhoum R, Martínez-Navarrete G, Corrochano S, et al. Functional and structural modifications during retinal degeneration in the rd10 mouse. *Neuroscience*. 2008;155(3):698–713.
61. Chang B, Hawes NL, Pardue MT, et al. Two mouse retinal degenerations caused by missense mutations in the β-subunit of rod cGMP phosphodiesterase gene. *Vis Res*. 2007;47(5):624–633.
62. Martínez-Fernández De La Cámara C, Hernández-Pinto AM, Olivares-González L, et al. Adalimumab reduces photoreceptor cell death in a mouse model of retinal degeneration. *Sci Rep*. 2015;5:11764.
63. Roche SL, Wyse-Jackson AC, Gómez-Vicente V, et al. Progesterone attenuates microglial-driven retinal degeneration and stimulates protective fractalkine-CX3CR1 signaling. *PLoS One*. 2016;11(11):e0165197.
64. Anasagasti A, Lara-López A, Milla-Navarro S, et al. Inhibition of microRNA 6937 delays photoreceptor and vision loss in a mouse model of retinitis pigmentosa. *Pharmaceutics*. 2020;12(10):1–15.
65. Chang B, Hawes NL, Hurd RE, Davisson MT, Nusinowitz S, Heckenlively JR. Retinal degeneration mutants in the mouse. *Vis Res*. 2002;42(4):517–525.
66. Görlach A, Bertram K, Hudecova S, Krizanova O. Calcium and ROS: a mutual interplay. *Redox Biol*. 2015;6:260–271.
67. Power M, Das S, Schütze K, Marigo V, Ekström P, Paquet-Durand F. Cellular mechanisms of hereditary photoreceptor degeneration—focus on cGMP. *Prog Retin Eye Res*. 2020;74:100772.
68. Tang TH, Chang CT, Wang HJ, et al. Oxidative stress disruption of receptor-mediated calcium signaling mechanisms. *J Biomed Sci*. 2013;20(1):48.
69. Chen Y, Perusek L, Maeda A. Autophagy in light-induced retinal damage. *Exp Eye Res*. 2016;144:64–72.
70. Naash MI, Ripps H, Li S, Goto Y, Peachey NS. Polygenic disease and retinitis pigmentosa: albinism exacerbates photoreceptor degeneration induced by the expression of a mutant opsin in transgenic mice. *J Neurosci*. 1996;16(24):7853–7858.
71. Wu L, Ueda K, Nagasaki T, Sparrow JR. Light damage in Abca4 and Rpe65rd12 Mice. *Invest Ophthalmol Vis Sci*. 2014;55(3):1910–1918.
72. Otsuka Y, Imamura K, Oishi A, et al. Phototoxicity avoidance is a potential therapeutic approach for retinal dystrophy caused by EYS dysfunction. *JCI Insight*. 2024;9(8):e174179.
73. Maeda A, Maeda T, Imanishi Y, et al. Retinol dehydrogenase (RDH12) protects photoreceptors from light-induced degeneration in mice. *J Biol Chem*. 2006;281(49):37697–37704.
74. Johnson K, Grawe F, Grzeschik N, Knust E. Drosophila crumbs is required to inhibit light-induced photoreceptor degeneration. *Curr Biol*. 2002;12(19):1675–1680.
75. Bighinati A, Adani E, Stanzani A, D'Alessandro S, Marigo V. Molecular mechanisms underlying inherited photoreceptor degeneration as targets for therapeutic intervention. *Front Cell Neurosci*. 2024;18:1343544.
76. Donovan M, Carmody RJ, Cotter TG. Light-induced photoreceptor apoptosis in vivo requires neuronal nitric-oxide synthase and guanylate cyclase activity and is caspase-3-independent. *J Biol Chem*. 2001;276(25):23000–23008.
77. Athanasiou D, Aguilà M, Bevilacqua D, Novoselov SS, Parfitt DA, Cheetham ME. The cell stress machinery and retinal degeneration. *FEBS Lett*. 2013;587(13):2008–2017.
78. Cronin T, Lyubarsky A, Bennett J. Dark-rearing the rd10 mouse: implications for therapy. *Adv Exp Med Biol*. 2012:723:129–136.
79. Arnault E, Barrau C, Nanteau C, et al. Phototoxic action spectrum on a retinal pigment epithelium model of age-related macular degeneration exposed to sunlight normalized conditions. *PLoS One*. 2013;8(8):e71398.
80. Thebeau C, Zhang S, Kolesnikov A V., Kefalov VJ, Semenkovich CF, Rajagopal R. Light deprivation reduces the severity of experimental diabetic retinopathy. *Neurobiol Dis*. 2020;137:104754.
81. Nakazawa M. Effects of calcium ion, calpains, and calcium channel blockers on retinitis pigmentosa. *J Ophthalmol*. 2011;2011:1–7.
82. Das S, Popp V, Power M, et al. Redefining the role of Ca2+-permeable channels in photoreceptor degeneration using diltiazem. *Cell Death Dis*. 2022;13(1):1–13.
83. Pantaleão SQ, Fernandes PO, Gonçalves JE, Maltarollo VG, Honorio KM. Recent advances in the prediction of pharmacokinetics properties in drug design studies: a review. *ChemMedChem*. 2022;17(1):e202100542.
84. Sánchez-Cruz A, Villarejo-Zori B, Marchena M, et al. Modulation of GSK-3 provides cellular and functional neuroprotection in the rd10 mouse model of retinitis pigmentosa. *Mol Neurodegener*. 2018;13(1):19.
85. Vighi E, Trifunovic D, Veiga-Crespo P, et al. Combination of cGMP analogue and drug delivery system provides functional protection in hereditary retinal degeneration. *Proc Natl Acad Sci USA*. 2018;115(13):E2997–E3006.
86. Roy A, Tolone A, Hilhorst R, Groten J, Tomar T, Paquet-Durand F. Kinase activity profiling identifies putative downstream targets of cGMP/PKG signaling in inherited retinal neurodegeneration. *Cell Death Discov*. 2022;8(1):93.

Investigative Ophthalmology & Visual Science